Assimilation of Surface Current Measurements in a Coastal Ocean Model

R. K. SCOTT, J. S. ALLEN, G. D. EGBERT, AND R. N. MILLER

College of Oceanic and Atmospheric Sciences, Oregon State University, Corvallis, Oregon

(Manuscript received 21 December 1998, in final form 18 November 1999)

ABSTRACT

An idealized, linear model of the coastal ocean is used to assess the domain of influence of surface type data, in particular how much information such data contain about the ocean state at depth and how such information may be retrieved. The ultimate objective is to assess the feasibility of assimilation of real surface current data, obtained from coastal radar measurements, into more realistic dynamical models. The linear model is used here with a variational inverse assimilation scheme, which is optimal in the sense that under appropriate assumptions about the errors, the maximum possible information is retrieved from the surface data. A comparison is made between strongly and weakly constrained variational formulations. The use of a linear model permits significant analytic progress. Analysis is presented for the solution of the inverse problem by expanding in terms of representer functions, greatly reducing the dimension of the solution space without compromising the optimization. The representer functions also provide important information about the domain of influence of each data point, about optimal location and resolution of the data points, about the error statistics of the inverse solution itself, and how that depends upon the error statistics of the data and of the model. Finally, twin experiments illustrate how well a known ocean state can be reconstructed from sampled data. Consideration of the statistics of an ensemble of such twin experiments provides insight into the dependence of the inverse solution on the choice of weights, on the data error, and on the sampling resolution.

1. Introduction

The capabilities of land-based high-frequency (HF) radar systems to produce maps of surface currents in coastal regions and the tremendous potential of these measurements to increase understanding of coastal ocean behavior are becoming increasingly well recognized (e.g., see Paduan and Graber 1997; Kosro et al. 1997; and other papers in the Special Issue on High Frequency Radars for Coastal Oceanography, *Oceanography*, **10**). Typically, these surface current maps extend over regions with horizontal scales of 20–50 km, with resolution of 1–2 km, and are available at time intervals of 20–60 min. Although the spatial and temporal coverage of these measurements provide a great amount of information on the state of the coastal ocean, that information is limited to the surface. It is natural, consequently, to enquire how that extensive surface information might be utilized together with a coastal ocean circulation model to give more information about the time-dependent subsurface flow. Motivated by that consideration, Lewis et al. (1998) developed and applied a nudging technique to assimilate HF radar surface current measurements into numerical ocean models. Here we take an alternative, theoretical approach in an effort to investigate some basic issues concerning assimilation of surface current measurements.

To do this we consider an idealized linear model of the coastal ocean and apply a formal inverse approach. Our general objective is to determine how much information at depth it is possible to obtain from knowledge of surface currents. That an inverse method approach is required stems from the ill-posed nature of the problem (illustrated in section 4 below) when knowledge of surface currents is incorporated directly into the model. One particular objective is to investigate exactly how the inverse method resolves the ill-posedness and to determine to what extent the resolution depends on the choice of weights used in the inverse method. A related issue is to determine how the choice of weights affect the agreement of the inverse solution with a given, known ocean state, in the case that the data used to obtain the inverse solution was obtained from that known state. In this example, knowledge of the surface current field will be obtained from an exact solution of the model equations and boundary conditions that form the well-posed forward problem. The inverse calculation will then attempt to reconstruct the exact solution of the forward problem when exact knowledge of one boundary condition is discarded and replaced by the additional knowledge of the surface current field.

Corresponding author address: Dr. John S. Allen, College of Oceanographic and Atmospheric Sciences, Oregon State University, 104 Ocean Admin. Bldg., Corvallis, OR 97331-5503.
E-mail: jallen@oce.orst.edu

The machinery for inverse calculations is already well established (e.g., Bennett 1992). However for most problems of practical significance, the expressions are too complicated to be solved analytically and numerical methods must be used. The model used in this study has the advantage that it allows analytic progress and still represents two important physical features of the coastal ocean: density stratification and friction, the latter through surface and bottom Ekman layers. One important feature that is not represented is realistic bottom topography.

2. Formulation of the forward model

We wish to consider an idealized model of the coastal ocean that represents enough physical features to be relevant and yet is simple enough to allow analytic progress. To achieve this we follow Allen (1973) and consider a two-dimensional, across-shelf slice of the ocean, that is, a slice that contains vertical and offshore dependence but no alongshore dependence. In particular we consider a rectangular domain with uniform depth H and offshore length L. The flow in such a domain is forced by a given alongshore wind stress that induces an across-shore Ekman transport and consequently an interior flow field.

We start with the evolution equations that describe an incompressible fluid satisfying the Boussinesq approximation on an f plane:

$$\frac{D}{Dt}\mathbf{u} + f\mathbf{k}\times\mathbf{u} = -\frac{1}{\rho_0}\nabla p - \frac{\rho}{\rho_0}g\mathbf{k} + \mathbf{F} \quad (2.1a)$$

$$\frac{D}{Dt}\rho = G \quad (2.1b)$$

$$\nabla\cdot\mathbf{u} = 0, \quad (2.1c)$$

where $\mathbf{u} = (u, v, w)$ is the velocity in $(x, y, z) \equiv$ (offshore, alongshore, vertical) coordinate space, p is the perturbation pressure, ρ is the density, ρ_0 is a constant reference density, $\mathbf{F}$ and G represent turbulent exchange processes, f is the Coriolis parameter, g is gravity, and $\mathbf{k} = (0, 0, 1)$.

We nondimensionalize the independent variables, x, y, z, t, by

$$(x, y) = L(x^*, y^*), \qquad z = Hz^*, \qquad t = f^{-1}t^*,$$

and the dependent variables u, v, w, p, ρ by

$$u = Uu^*, \qquad v = Uv^*, \qquad w = (H/L)Uw^*,$$

$$\rho = \rho_0 + \overline{\rho}(z) + \rho_0\frac{UfL}{gH}\rho^*$$

$$p = -\left[\rho_0 + \frac{1}{2}\overline{\rho}(z)\right]gHz^* + \rho_0 UfLp^*,$$

where U is a characteristic horizontal velocity and $\overline{\rho}(z)$ is a vertical density structure that depends linearly on z. It is assumed that U depends on the magnitude of the applied wind stress forcing through $U = \tau_0/\rho_0 fHE_V$, where τ_0 is a characteristic (dimensional) wind stress and $E_V = A_V/(fH^2)$ is the vertical Ekman number in which A_V is a constant vertical eddy coefficient.

To simplify (2.1a–c) we assume that the aspect ratio $H/L \ll 1$ so the motion is in approximate hydrostatic balance; that the Rossby number, $\mathrm{Ro} = U/fL$, is small so that nonlinear terms can be neglected; and that the horizontal and vertical Ekman numbers, E_H and E_V are small with $E_H \ll E_V \ll 1$ so viscous terms can be neglected (outside of surface and bottom boundary layers). We also assume that there is no alongshore, y, dependence. The resulting equations are (dropping the asterisks)

$$u_t - v = -p_x \quad (2.3a)$$

$$v_t + u = 0 \quad (2.3b)$$

$$\rho_t - Sw = 0 \quad (2.3c)$$

$$u_x + w_z = 0 \quad (2.3d)$$

$$0 = -p_z - \rho, \quad (2.3e)$$

where $S = N^2H^2/f^2L^2$ is a stratification parameter and $N^2 = -g\overline{\rho}_z/\rho_0$ is a constant.

The model is forced with a wind stress that varies harmonically in time with nondimensional frequency ω and nondimensional amplitude $\tau(x)$. The time dependence of all the model fields is also therefore harmonic with frequency ω. We consider only frequencies much smaller than the inertial frequency, $\omega \ll 1$. Balancing the terms in (2.3b) gives $u = O(\omega)v$, and consequently (2.3a) becomes

$$v = p_x. \quad (2.3a')$$

With the above assumptions the system (2.3a′,b–e) can be rewritten as a single equation for $p(x, z, t)$:

$$\frac{\partial}{\partial t}(p_{xx} + S^{-1}p_{zz}) = 0. \quad (2.4)$$

The boundary conditions at the coast ($x = 0$) and at the offshore boundary ($x = 1$) are no normal flow, $u = 0$. From (2.3a,b) with the above harmonic time-dependence, $u = 0$ is equivalent to the condition $p_x = 0$. The boundary conditions at the surface ($z = 1$) and bottom ($z = 0$) must take into account the surface and bottom Ekman layers of depth $O(E_V^{1/2})$ in the limit $E_V \ll 1$. Under the assumption $\omega \ll 1$ the Ekman layers may be regarded as quasi steady and their solutions give boundary conditions on the vertical velocity, w (Pedlosky 1987). At the surface, a rigid lid is assumed and the boundary condition is $w = E_V\tau_x$, where $\tau(x)$ is assumed to satisfy $\tau(0) = 1$, $\tau(1) = 0$. At the bottom, the Ekman layer resulting from the no slip condition gives $w = E_V^{1/2}v_x$.

Because of the approximations involved in representing the surface and bottom Ekman layers, modifi-

cation of the coastal and offshore boundary conditions is required. In particular, a concentrated inflow is required at $(x, z) = (0, 1)$ so that the boundary condition becomes $u = -E_V\delta(1 - z)$. Note that no such modification is required at the offshore boundary, $x = 1$, because $\tau(1) = 0$.

Reformulating the boundary conditions on w in terms of p_z using (2.3a′,c,e) and with the notation change $p(x, z, t) \rightarrow p(x, z)e^{i\omega t}$ for all dependent variables, we obtain

$$\begin{aligned} i\omega p_x &= 0 && \text{at } x = 1, \\ i\omega p_x &= E_V\delta(1 - z) && \text{at } x = 0, \qquad (2.5a) \\ i\omega p_z &= -SE_V^{1/2}p_{xx} && \text{at } z = 0, \\ i\omega p_z &= -SE_V\tau_x && \text{at } z = 1 \qquad (2.5b) \end{aligned}$$

together with

$$p_{xx} + S^{-1}p_{zz} = 0. \qquad (2.6)$$

Although it is possible to solve (2.6), (2.5a,b) directly, it is more instructive to consider the solution obtained by boundary layer methods, thereby isolating the relevant coastal dynamics (Allen 1973). In particular, when $S \ll 1$, there is a natural scale separation into an inner (coastal) region with horizontal length scale $O(S^{1/2})$, which is the dimensionless Rossby radius, and an outer (open ocean) region with horizontal length scale $O(1)$. In the outer region (2.3e) becomes at leading order

$$p_z = 0, \qquad (2.7)$$

decoupling (2.3c) from the remaining equations. The relevant boundary conditions for $x = O(1)$ are the surface and bottom conditions:

$$w = E_V^{1/2}v_x \quad \text{at } z = 0, \qquad w = E_V\tau_x \quad \text{at } z = 1. \qquad (2.8)$$

In terms of the velocities, the solution u_0, v_0, w_0 for $x = O(1)$ satisfying the surface and bottom boundary conditions is

$$u_0 = -E_V\tau\frac{i\omega}{E_V^{1/2} + i\omega} \qquad (2.9a)$$

$$v_0 = E_V\tau\frac{1}{E_V^{1/2} + i\omega} \qquad (2.9b)$$

$$w_0 = E_V\tau_x\frac{E_V^{1/2} + i\omega z}{E_V^{1/2} + i\omega}. \qquad (2.9c)$$

We have assumed implicitly that the vertically integrated u velocity is exactly balanced by the transport in the surface and bottom Ekman layers. Since $\tau(1) = 0$ the solution (2.9a–c) satisfies identically the boundary condition at the vertical offshore wall, $x = 1$, so there is no need for an additional boundary layer here. The boundary condition at the vertical coast, $x = 0$, on the other hand, is not satisfied since $\tau(0) = 1$.

To satisfy the boundary condition at $x = 0$ we use a boundary layer correction that satisfies the equations (2.3a′,b–e) for $x = O(S^{1/2}) \ll 1$ and such that at $x = 0$ the across-shore correction velocity, u', balances both the solution u_0 and the transport due to the surface and bottom Ekman layers. Such a balance will ensure no normal flow integrated over the full vertical extent of the coastal boundary, including the Ekman transports. In fact, it turns out that the transport at the coast due to the bottom Ekman layer is zero because at the coast/bottom corner $u(0, 0) = 0$ implies $v_t(0, 0) = 0$ and thus $v(0, 0) = 0$. It is therefore necessary to consider only the surface Ekman layer transport at the coast. Thus the boundary condition for the across-shore inner region correction velocity is

$$u = E_V\frac{i\omega}{E_V^{1/2} + i\omega} - E_V\delta(1 - z), \quad \text{at } x = 0. \qquad (2.10)$$

We now make the following rescaling, using primes to denote variables in the inner region:

$$\begin{aligned} &x = S^{1/2}x', \quad z = z', \quad \omega = E_V^{1/2}\omega', \\ &u = E_Vu', \quad v = E_V^{1/2}v', \quad w = E_VS^{-1/2}w', \\ &\rho = E_V^{1/2}S^{1/2}\rho', \quad p = E_V^{1/2}S^{1/2}p'. \end{aligned}$$

Under this scaling, the governing equations in the inner region, or coastal boundary layer, become

$$-v' = -p'_{x'} \qquad (2.12a)$$

$$i\omega'v' + u' = 0 \qquad (2.12b)$$

$$i\omega'\rho' - w' = 0 \qquad (2.12c)$$

$$u'_{x'} + w'_{z'} = 0 \qquad (2.12d)$$

$$0 = -p'_{z'} - \rho', \qquad (2.12e)$$

and the equation for the pressure becomes

$$p'_{x'x'} + p'_{z'z'} = 0. \qquad (2.13)$$

The relevant boundary conditions become

$$\begin{aligned} i\omega'p'_{x'} &= \frac{i\omega'}{1 + i\omega'} + \delta(1 - z') && \text{at } x' = 0, \\ i\omega'p'_{x'} &\rightarrow 0 && \text{at } x' \rightarrow \infty; \qquad (2.14a) \\ i\omega'p'_{z'} &= -p'_{x'x'} && \text{at } z' = 0, \\ i\omega'p'_{z'} &= 0 && \text{at } z' = 1. \qquad (2.14b) \end{aligned}$$

Here $x' \rightarrow \infty$ represents the limit in which the outer solution is valid.

3. The inner solution

From here on we shall be concerned mainly with the flow in the coastal boundary layer, or inner region. Matching the flow in the outer region, with the flow in the inner region at the coast provides the coastal boundary condition for the inner region solution, as described

above. The domain of the inner region is specified as follows. The vertical coordinate is z' with $z' = 0$ at the bottom and $z' = 1$ at the surface. The across-shore coordinate is x' with $x' = 0$ at the coast and $x' \to \infty$ in the outer region.

Rather than solve (2.13), (2.14a,b) directly, it is more convenient to work in one or other of the two frequency limits, $\omega' \gg 1$ or $\omega' \ll 1$. In the following we shall restrict attention to the case $\omega' \gg 1$, which corresponds to a surface Ekman layer transport that is balanced by an interior across-shelf transport. The balance is on a shorter timescale than the spindown timescale for the interior flow, so no bottom Ekman layer is present. (The resulting implied frequency range for ω is $1 \gg \omega \gg E_V^{1/2}$.) In this case, taking the x derivative of (2.13), and absorbing the factor of $i\omega'$ in (2.14a,b) by the rescaling $v = p_x = i\omega' p_x'$ and dropping the primes on the other variables, we obtain

$$v_{xx} + v_{zz} = 0 \tag{3.1}$$

$$\begin{aligned} v &= -1 + \delta(1 - z) && \text{at } x = 0, \\ v &\to 0 && \text{at } x \to \infty, \\ v_z &= 0 && \text{at } z = 0, 1 \end{aligned} \tag{3.2}$$

with the solution, obtained by Fourier expanding in the vertical,

$$v = 2 \sum_{n=1}^{\infty} (-1)^n e^{-n\pi x} \cos n\pi z \tag{3.3a}$$

$$= \frac{-e^{-\pi x} - \cos \pi z}{\cosh \pi x + \cos \pi z}. \tag{3.3b}$$

Note that ρ, and hence w, can be recovered from (3.3a) by use of the relation $v_z = -\rho_x$ and the condition $\rho \to 0$ at $x \to \infty$.

In section 7 we will use a version of (3.3a) that is not singular at the coast/surface corner. Namely, we replace the coastal boundary condition in (3.2) with a limiting form $v(0, z) = -1 + \delta^{(k)}(1 - z)$, where

$$\delta^{(k)}(z) = \begin{cases} k, & \text{if } |z| \le \dfrac{1}{k} \\ 0, & \text{otherwise.} \end{cases} \tag{3.4}$$

The solution (3.3a) then becomes

$$v^{(k)} = -2 \sum_{n=1}^{\infty} (-1)^n \frac{k}{n\pi} \sin \frac{n\pi}{k} e^{-n\pi x} \cos n\pi z. \tag{3.5}$$

This solution $v^{(k)}$ will be considered as the baroclinic part of the ''true ocean state'' used in section 7. See also appendix A for a discussion of how the barotropic and baroclinic parts of any given data may be separated in this boundary layer formulation.

4. The ill-posed data problem

Now suppose that we have additional surface current information, or data. Real data obtained from HF radar measurements typically represents currents in the top meter of water. In this study, however, the relevant surface boundary condition requires knowledge of the surface currents below the Ekman layer. We assume here, therefore, that the Ekman layer can be solved exactly to provide surface currents below the Ekman layer in terms of the measured surface currents above. We also assume that data for the inner variables is provided over the entire inner region, that is, out to distances greater than the Rossby radius. Since by (2.12b) and the assumption $\omega' \gg 1$ we have that $v \gg u$ in the inner region, we obtain an additional boundary condition for (3.1) of the form

$$v = d(\chi) \quad \text{at } z = 1, \tag{4.1}$$

which makes the problem overspecified. When indexing data (and the data representers in sections 5–7 below), we will typically use the Greek letters χ, η, etc., to denote the independent variable along the surface, with $\chi = 0$ at the coast and $\chi \to \infty$ in the outer region.

Recall now that the coastal boundary condition on v_x was derived from matching the inner region across-shore velocity u' with the outer region across-shore velocity u_0. Thus the coastal boundary condition for the inner problem is based upon what we know about the velocity field in the outer region, and in practice it is likely that this information will be only poorly known. Thus, the coastal boundary condition will be the least reliable of all the boundary conditions for the inner problem and therefore will be the natural choice to relax. If we completely discard the boundary condition at the coast in (3.2) the problem becomes one of solving an elliptic equation, (3.1), with both Dirichlet and Neumann conditions on one boundary segment and no conditions on another boundary segment. Such a problem is typically ill-posed: if a unique solution exists, then it is unstable to small perturbations of the boundary conditions (Hadamard 1952). To illustrate, we formally construct the ill-posed solution to (3.1) with the boundary conditions (3.2) and (4.1), but omitting the boundary condition at $x = 0$, and demonstrate that the solution is unstable. In terms of v, we have

$$\nabla^2 v = 0, \tag{4.2}$$

$$v \to 0 \quad \text{at } x \to \infty, \qquad v_z = 0 \quad \text{at } z = 0, 1 \tag{4.3a}$$

$$v = d(\chi) \quad \text{at } z = 1. \tag{4.3b}$$

The solution is

$$v(x, z) = \sum_{n=1}^{\infty} B_n e^{-n\pi x} \cos n\pi z, \tag{4.4}$$

where the B_n must satisfy

$$\sum_{n=1}^{\infty} B_n e^{-n\pi\chi} (-1)^n = d(\chi). \tag{4.5}$$

We now require that $d(\chi)$ is finite and continuous for $\chi \in [0, \infty)$ so that the sequence of partial sums of the form

(4.5) converge uniformly in χ. Further, we assume that the barotropic component of the data has already been removed (see appendix A) and so we require $d(\chi) \to 0$ as $\chi \to \infty$. Multiplying (4.5) by $e^{-m\pi\chi}$ and integrating over $[0, \infty)$ gives

$$\sum_{n=1}^{\infty} B'_n \frac{1}{n+m} = \int_0^{\infty} d(x) e^{-m\pi x}\, dx = \tilde{d}_m, \quad (4.6)$$

where $B'_n = B_n(-1)^n/\pi$. This can be written as an infinite matrix product

$$\mathbf{H}\mathbf{B}' = \tilde{\mathbf{d}}, \quad (4.7)$$

where $\mathbf{B}' = (B'_1, B'_2, \cdots)^{\mathrm{T}}$, $\tilde{\mathbf{d}} = (\tilde{d}_1, \tilde{d}_2, \cdots)^{\mathrm{T}}$, the superscript T denotes transpose, and $\mathbf{H}$ is the infinite Hilbert matrix, given by $H_{mn} = (m+n)^{-1}$, that is,

$$\mathbf{H} = \begin{pmatrix} \frac{1}{2} & \frac{1}{3} & \frac{1}{4} & \\ \frac{1}{3} & \frac{1}{4} & \frac{1}{5} & \\ \frac{1}{4} & \frac{1}{5} & \frac{1}{6} & \\ & & & \ddots \end{pmatrix}. \quad (4.8)$$

One of the properties of the infinite Hilbert matrix is that it does not have a formal matrix inverse, so direct inversion of (4.7) is not possible. In fact even for the finite dimensional $N \times N$ matrix, which has a well-defined matrix inverse, $[\mathbf{H}^{(N)}]^{-1}$, the determinant of $\mathbf{H}^{(N)}$ tends rapidly to zero as N becomes even moderately large; for example, for $N = 10$, $\det(\mathbf{H}^{(10)}) \approx 10^{-58}$, which is beyond the limit of current computer accuracy. We note however that $\mathbf{H}$ can be written in the form $\mathbf{H} = \mathbf{A}\mathbf{A}^{\mathrm{T}}$, where $\mathbf{A}$ is a lower triangular infinite matrix with a well-defined formal inverse $\mathbf{E} = \mathbf{A}^{-1}$ (e.g., Choi 1983). It follows that

$$\mathbf{H}\mathbf{B}' = \tilde{\mathbf{d}} \Rightarrow \mathbf{B}' = \mathbf{E}^{\mathrm{T}}(\mathbf{E}\tilde{\mathbf{d}}), \quad (4.9)$$

where the formal matrix multiplications on the rhs are well-defined. (Note that $\mathbf{E}^{\mathrm{T}}\mathbf{E}$ is not defined and that infinite matrix multiplication is not associative.) Thus although (4.9) implies a unique solution of (4.7), the lack of a well-defined matrix inverse of $\mathbf{H}$ means that the solution must necessarily be unstable to small perturbations of the data, $\tilde{\mathbf{d}}$. The instability is a manifestation of the ill-posed nature of solving an elliptic equation with both Dirichlet and Newman boundary conditions on a single boundary segment.

5. Resolution by a variational formulation (strongly constrained)

To resolve difficulties associated with ill-posedness, while still taking into account the extra information available from knowledge of the surface velocity, we consider formulation of an inverse problem. We assume that the surface data is inexact, that is, that there are data errors and that we also have some inexact information about the across-shore velocity field at the coastal boundary. We then seek an ''inverse solution'' that minimizes a measure of the data errors on the surface and the velocity field errors at the coast. The actual form of the measure, for example the relative importance, or ''weight,'' given to the surface data compared to the coastal boundary condition, or the nature of the coastal boundary condition itself, will depend upon our particular requirements for the inverse solution.

One possibility is that the across-shore velocity at the coastal boundary is in some sense small. Recalling (2.12b), this gives a boundary condition on the alongshore velocity v of the form

$$v = 0 + \varepsilon(z) \quad \text{at } x = 0, \quad (5.1)$$

where ε represents the errors in this assumption. We then minimize a ''penalty functional,'' $\mathcal{T}[v]$, that depends on the data errors $\delta = v - d$ at the surface and on the boundary condition error ε at the coast:

$$\mathcal{T}[v] = w_c \int_0^1 dz' \varepsilon^2 + w_d \int_0^{\infty} d\chi \delta^2, \quad (5.2)$$

where w_c and w_d are weights and where the terminology data errors includes observational errors as well as other sources of model–data misfit.

In summary, our inverse solution is the unique solution to the following system

$$\nabla^2 v = 0, \quad (5.3)$$

$$v = \varepsilon(z) \quad \text{at } x = 0,$$

$$v \to 0 \quad \text{at } x \to \infty,$$

$$v_z = 0 \quad \text{at } z = 0, 1 \quad (5.4a)$$

$$v = d(\chi) + \delta(\chi) \quad \text{at } z = 1 \quad (5.4b)$$

that minimizes the penalty functional (5.2). Note that for consistency we make the further assumption on ε that

$$\int_0^1 \varepsilon(z)\, dz = 0 \quad (5.5)$$

and the assumptions on the data and data error that $d \to 0$ and $\delta \to 0$ as $x \to \infty$. This is equivalent to considering only the baroclinic part of the data and resulting inverse solution. See appendix A for details of how the barotropic and baroclinic parts are separated.

The data error at the surface, $\delta(\chi)$, and the value of v at the coast, $\varepsilon(z)$ are not known a priori, but rather are uniquely determined by requiring that the inverse solution minimizes $\mathcal{T}$. Note that $\mathcal{T}$ represents the departure in a weighted least squares sense of the inverse solution from the surface data with weight w_d, and from the coastal information with weight w_c. Generalization of the weights to take into account the covariances of

data or boundary condition errors at one point with those at another point complicates the analysis and is not essential to the main theme of this paper.

In the above formulation we treat the model equation (5.3) and the other boundary conditions at $x \to \infty$, $z = 0$ and $z = 1$ in (5.4a) as exact, motivated by the specific objective of determining how the inverse problem resolves difficulties with ill-posedness discussed in section 4. As a result, the inverse problem is strongly constrained by the model equations. It is possible to relax these conditions by the addition of suitable terms to the penalty functional to allow for errors in the model equations. This weak constraint generalization, in which model errors are included, is considered in section 6.

Our method of solution of the inverse problem utilizes an expansion of the inverse solution in terms of ''representer functions'' (see, e.g., Bennett 1992, sections 5.4–5.5 for an introduction). In addition to providing the solution, the representer functions and the associated representer matrix provides information about the range of influence of data at a particular location. An alternative method of solution, which utilizes a Fourier series expansion, is outlined in appendix A. Although it provides less information about data influence, it enables a more direct minimization of $\mathcal{T}$ without the need for functional variation.

The penalty function, $\mathcal{T}$, is completely determined by the value of v at the coast, $x = 0$. That is, given $\varepsilon(z) = v(0, z)$, and temporarily dropping the other condition (5.4b), we have a well-defined problem with a unique solution. We call this well-defined problem, the undetermined forward problem, undetermined because we do not yet know which realization of ε will lead to the minimization of $\mathcal{T}$. Explicitly, the undetermined forward problem is specified uniquely by (5.3) with (5.4a). Given a particular realization of ε we uniquely determine $v(x, z)$ and hence the $v(\chi, 1)$ that appears in the second integral of (5.2). [Note that the forward problem in the usual sense is given by setting $\varepsilon \equiv 0$ and has solution $v(x, z) \equiv 0$.]

We can construct the solution to (5.3), (5.4a) in terms of the Green's function:

$$v(x, z) = \int_0^1 dz' \gamma(x, z; z')\varepsilon(z'), \tag{5.6}$$

where the Green's function $\gamma(x, z; z')$ satisfies

$$\nabla^2\gamma = 0 \tag{5.7}$$

$$\gamma = \delta(z - z') - 1 \quad \text{at } x = 0,$$
$$\gamma \to 0 \quad \text{at } x \to \infty,$$
$$\gamma_z = 0 \quad \text{at } z = 0, 1. \tag{5.8}$$

The system (5.7, 5.8) can be solved analytically:

$$\gamma(x, z; z') = 2\sum_{n=1}^{\infty} e^{-n\pi x} \cos n\pi z \cos n\pi z' \tag{5.9a}$$

$$= \frac{1}{2}\left[\frac{\cos\pi(z + z') - e^{-\pi x}}{\cosh\pi x - \cos\pi(z + z')} + \frac{\cos\pi(z - z') - e^{-\pi x}}{\cosh\pi x - \cos\pi(z - z')}\right]. \tag{5.9b}$$

We now establish a set of functions, the representer functions, that will provide a natural basis in which to express the solution that minimizes the penalty functional. First we define an inner product over the coastal domain $(0, z')$ by

$$\langle u, v\rangle_c = \int_0^1 dz' u(z')v(z'), \tag{5.10}$$

which enables us to write (5.6) as

$$v(x, z) = \langle\gamma(x, z; z'), \varepsilon(z')\rangle_c = \langle\gamma(x, z; \cdot), \varepsilon\rangle_c. \tag{5.11}$$

The inner product provides a Hilbert space structure, H, over the vector space of continuous functions on [0, 1]. Setting $z = 1$ in (5.11) shows that for each fixed χ the function $r_0(\chi; z') = \gamma(\chi, 1; z')$ (an element of the Hilbert space of coastal boundary conditions H) is the representer associated with the surface data point χ (e.g., Renardy and Rogers 1993, section 6.3). That is, for $\chi \in [0, \infty)$, $r_0(\chi; z')$ is the unique function in H satisfying

$$v(\chi, 1) = \langle r_0(\chi; \cdot), \varepsilon\rangle_c, \tag{5.12}$$

for arbitrary ε in H, with v and ε related through (5.3) and (5.4a). Thus, (5.2) can be rewritten using the inner product and representer functions in the integrand:

$$\mathcal{T}[v] = \mathcal{T}[\varepsilon] = w_c\langle\varepsilon, \varepsilon\rangle_c + w_d\int_0^{\infty} d\chi|\langle r_0(\chi; \cdot), \varepsilon\rangle_c - d(\chi)|^2. \tag{5.13}$$

With the penalty functional written in the form (5.13), it can be shown (Bennett 1992; or appendix B here) that the undetermined boundary condition $\varepsilon(z)$ that minimizes $\mathcal{T}[\varepsilon]$ can be written in the form

$$\varepsilon(z) = \int_0^{\infty} d\chi\nu(\chi)r_0(\chi, z), \tag{5.14}$$

where $\nu(\chi)$ satisfies

$$\int_0^{\infty} d\chi\nu(\chi)[R(\chi, n) + c\delta(\chi - \eta)] = d(\eta), \tag{5.15}$$

with the representer kernel $R(\chi, \eta)$ defined by

$$R(\chi, \eta) = \langle r_0(\chi, \cdot), r_0(\eta, \cdot)\rangle_c, \tag{5.16}$$

and where $c = w_c/w_d$. The analysis leading to this result is a straightforward extension of that described in Ben-

nett (1992), from the case with discrete data to the case of continuous data. For completeness, we outline the procedure in appendix B; see also Bennett (1992, chapter 8). In (5.14) and (5.15) we have used the fact that the forward solution, that is, the solution to the system (5.3), (5.4a) with $\epsilon \equiv 0$, is identically zero. This is in accordance with only assuming that the value of v on the coast is small and assuming nothing about the vertical structure of v on the coast.

As noted above, the solution in the full model domain is completely determined once $\varepsilon(z)$ is known. It follows from (5.14) and (5.6) that the unique inverse solution $\hat{v}(x, z)$ that minimizes (5.2) and satisfies (5.3)–(5.5) is

$$\hat{v}(x, z) = \int_0^\infty d\chi \nu(\chi) r_c(\chi; x, z), \tag{5.17}$$

where we define

$$r_c(\chi; x, z) = \langle \gamma(x, z; \cdot), r_0(\chi, \cdot) \rangle_c. \tag{5.18}$$

Note that $r_c(\chi; x, z)$ is just the solution to (5.3) with the coastal boundary condition in (5.4a) set to $r_0(\chi, z)$. For consistency with the weak constraint case considered in section 6 we refer to the functions $r_c(\chi; x, z)$ as the representers, although more precisely the designation should be applied to the closely related functions $r_0(\chi; z)$.

With the explicit expression (5.9a) for the Green's function, (5.18) and (5.16) give respectively

$$r_c(\chi; x, z) = 2 \sum_{n=1}^\infty e^{-n\pi(x+\chi)}(-1)^n \cos n\pi z \tag{5.19a}$$

$$= \frac{-e^{-\pi(x+\chi)} - \cos\pi z}{\cosh\pi(x + \chi) + \cos\pi z}, \tag{5.19b}$$

$$R(\chi, \eta) = 2 \sum_{n=1}^\infty e^{-n\pi(\chi+\eta)} \tag{5.20a}$$

$$= 2\frac{e^{-\pi(\chi+\eta)}}{1 - e^{-\pi(\chi+\eta)}}. \tag{5.20b}$$

The representer functions provide a useful indication of the relative influence of data at a particular location on the inverse solution. For example, for a given χ, relatively large values of $r_c(\chi; x, z)$ indicate that the inverse solution has significant dependence on the data at χ, whereas near-zero values of $r_c(\chi; x, z)$ indicate that the solution has negligible dependence on the data at χ; that is, the data at χ do not influence the solution at locations where $r_c(\chi; x, z)$ is small. Further discussion is given in section 7a.

A closed form analytic solution for the inverse solution, $\hat{v}(x, z)$, requires the determination of the function $\nu(\chi)$ and hence the inversion of the integral equation (5.15). The problem of the inversion of (5.15) can be reduced to a problem involving an infinite matrix. The approach is to consider the Fourier series representation of the inverse solution (5.17), that is, to write

$$\hat{v}(x, z) = \sum_{n=1}^\infty \overline{v}_n (-1)^n e^{-n\pi x} \cos n\pi z, \tag{5.21}$$

where the factor of $(-1)^n$ has been included for later convenience. Substituting the expression (5.19a) for $r_c(\chi; x, z)$ into the solution (5.17) we have

$$\hat{v}(x, z) = \int_0^\infty d\chi \nu(\chi) 2 \sum_{n=1}^\infty e^{-n\pi(x+\chi)}(-1)^n \cos n\pi z. \tag{5.22}$$

Since the series is uniformly convergent in χ, we can exchange integral and sum. Comparing (5.21) and (5.22) we see that

$$\overline{v}_n = 2 \int_0^\infty d\chi \nu(\chi) e^{-n\pi\chi}. \tag{5.23}$$

Using (5.20a), (5.15) is

$$\int_0^\infty d\chi \nu(\chi) \left[2 \sum_{n=1}^\infty e^{-n\pi(x+\chi)} + c\delta(\chi - \eta) \right] = d(\eta). \tag{5.24}$$

Multiplying both sides by $e^{-m\pi\eta}$ and integrating over $[0, \infty)$ with respect to η gives

$$2 \sum_{n=1}^\infty \frac{1}{(m + n)\pi} \int_0^\infty d\chi \nu(\chi) e^{-n\pi\chi} \tag{5.25}$$

$$+ c \int_0^\infty d\chi \nu(\chi) e^{-m\pi\chi} = \int_0^\infty d\eta d(\eta) e^{-m\pi\eta} \equiv \tilde{d}_m. \tag{5.26}$$

Finally, substituting $\overline{v}_n$ from (5.23) for the integrals on the lhs of (5.25) gives

$$\sum_{n=1}^\infty \left[\frac{1}{(m + n)\pi} + \frac{c}{2}\delta_{mn} \right] \overline{v}_n = \tilde{d}_m. \tag{5.27}$$

As in section 4, this can be written as an infinite matrix product:

$$(\mathbf{H} + \mathbf{C})\overline{\boldsymbol{v}} = \pi\mathbf{d}, \tag{5.28}$$

where $\mathbf{C}$ is defined by

$$C_{mn} = \frac{\pi}{2} c \delta_{mn} = \left(\frac{w_c}{w_d} \right) \frac{\pi}{2} \delta_{mn}$$

and otherwise with the same notation convention as section 4. The difference here is that the infinite matrix, $\mathbf{H} + \mathbf{C}$, has a well-defined inverse because of the extra diagonal entries. Thus (5.28) can be inverted to give an expression for $\overline{\boldsymbol{v}}$ and therefore for each $\overline{v}_n$, that is stable to small perturbations of $\tilde{\mathbf{d}}$. In the limit of infinite data weight, $c = w_c/w_d \to 0$ and the ill-posed expression (4.7) is recovered. In the limit of zero data weight, $c \to \infty$ and we have $\overline{v}_n \equiv 0$; that

is, the velocity at the coast, ε, is minimized unconditionally to zero.

6. The weakly constrained variational problem

We now consider a variational formulation that takes into account the errors in the model dynamics. As a notational shorthand we use the following convention for integrations over the whole domain:

$$\int_D u = \int_0^\infty dx \int_0^1 dz u(x, z). \tag{6.1}$$

Similarly, integrations over the surface are written $\int_S u = \int_0^\infty d\chi\ u(\chi, 1)$ and integrations over the coast are written $\int_C u = \int_0^1 dz\, u(0, z)$. In cases of ambiguity, we use subscripts to indicate the variable of integration: $\int_{S_\eta} Ku = \int_S d\eta\ K(\chi, \eta) u(\eta, 1) = \int_0^\infty d\eta\ K(\chi, \eta) u(\eta, 1)$.

The simplest approach for a weakly constrained variational problem, allowing for model errors, is to use the system (5.3) and (5.4a,b) but with $\nabla^2 v = 0$ replaced by

$$\nabla^2 v = \varphi \tag{6.2}$$

and then to minimize the penalty functional defined by

$$\mathcal{T}[v] = w_m \int_D \varphi^2 + w_c \int_C \varepsilon^2 + w_d \int_S \delta^2. \tag{6.3}$$

This provides the solution $\hat{v}$ closest to the exact model, the coastal boundary condition and the data. One drawback with this formulation is that by representing all the different model errors in the single scalar φ our inverse solution only provides us with the alongshore velocity field $\hat{v}$ and we cannot recover the other fields self-consistently. (See appendix C for discussion of an alternative approach.) Since we can achieve our objective involving comparison of the strong and weak constraint formulations by considering the alongshore velocity alone we adopt the simplest approach.

Thus, the inverse solution is the unique solution to (6.2) with boundary conditions

$$v \to 0 \qquad \text{at } x \to \infty,$$
$$v_z = 0 \qquad \text{at } z = 0, 1; \tag{6.4a}$$
$$v = \varepsilon(z) \qquad \text{at } x = 0,$$
$$v = d(\chi) + \delta(\chi) \qquad \text{at } z = 1 \tag{6.4b}$$

that minimizes (6.3).

Consistent with our treatment of the strong constraint problem, we note that we can treat the barotropic and baroclinic parts separately and insist upon the further conditions

$$\int_0^1 \varepsilon(z)\, dz = 0 \quad \text{and} \quad \int_0^1 \varphi(x, z)\, dz = 0, \tag{6.5}$$

for every x.

The method of solution is similar to that used in section 5 for the strong constraint problem. First we define an inner product by

$$(u, v) = w_m \int_D (\nabla^2 u)(\nabla^2 v) + w_c \int_C uv \tag{6.6}$$

so that we can write $\mathcal{T}$ as

$$\mathcal{T}[v] = (v, v) + w_d \int_S (v - d)^2. \tag{6.7}$$

By a procedure similar to that used in section 5, outlined in appendix B, the solution that minimizes (6.7) is then given by

$$\hat{v} = \int_{S_\chi} \nu r, \tag{6.8}$$

where $r(\chi) = r(\chi; x, z)$, defined uniquely by

$$v(\chi, 1) = (r(\chi; \cdot), v), \tag{6.9}$$

is the representer associated with the data point $(x, z) = (\chi, 1)$, and where $\nu = \nu(\chi,)$ are the representer coefficients satisfying

$$\int_{S_\eta} \nu(\eta)[R(\eta, \chi) + w_d^{-1}\delta(\eta - \chi)] = d(\chi). \tag{6.10}$$

Here $R = R(\chi, \eta)$ is the representer kernel defined by

$$R(\chi, \eta) = (r(\chi; \cdot), r(\eta; \cdot)) = r(\chi; \eta, 1). \tag{6.11}$$

With the restrictions (6.5) it can be shown (appendix B) that the representer functions, $r(\chi)$, defined by (6.9) satisfy the following system

$$\nabla^2 r = w_m^{-1} r^\dagger \tag{6.12}$$

$$r = -w_c^{-1} r_x^\dagger \quad \text{at } x = 0, \qquad r \to 0 \quad \text{at } x \to \infty,$$
$$r_z = 0 \qquad \text{at } z = 0, 1, \tag{6.13}$$

where the adjoint representer functions, $r^\dagger$, satisfy

$$\nabla^2 r^\dagger = \delta(\chi - x)[\delta(1 - z) - 1] \tag{6.14}$$

$$r^\dagger = 0 \quad \text{at } x = 0, \qquad r^\dagger \to 0 \quad \text{at } x \to \infty,$$
$$r_z^\dagger = 0 \quad \text{at } z = 0, 1. \tag{6.15}$$

As in section 5 we define the undetermined forward problem by the system (6.2) with the first four boundary conditions of (6.4a,b), that is without the boundary condition associated with the data. Again, this system has a solution in terms of a Green's function:

$$v(x, z) = \int_D dx'\ dz' G(x, z; x', z')\varphi(x', z') - \int_C dz' G_{x'}(x, z; 0, z')\varepsilon(z'), \tag{6.16}$$

where the Green's function, $G(x, z; x', z')$, satisfies

$$\nabla^2 G = \delta(x - x')[\delta(z - z') - 1] \tag{6.17}$$

$$G = 0 \quad \text{at } x = 0, \qquad G \to 0 \quad \text{at } x \to \infty,$$

$$G_z = 0 \quad \text{at } z = 0, 1. \tag{6.18}$$

Note that the strong constraint solution (5.6) is recovered in the special special case $\varphi = 0$, with the identification $G_{x'}(x, z; 0, z') = -\gamma(x, z; z')$.

Comparison of the Green's function system (6.17), (6.18) with the adjoint representer system (6.14), (6.15) shows that the adjoint representer functions satisfy

$$r^\dagger(\chi; x, z) = G(x, z; \chi, 1). \tag{6.19}$$

Similarly, comparison of the undetermined forward problem (6.2), (6.4a,b) with the representer system (6.12), (6.13) shows that the representer functions can be written, analogously to (6.16), in the form

$$r(\chi; x, z) = w_m^{-1} \int_D dx'dz' G(x, z; x', z') r^\dagger(\chi; x', z') + w_c^{-1} \int_C dz' G_{x'}(x, z; 0, z') r^\dagger_{x'}(\chi; 0, z'). \tag{6.20}$$

Substituting (6.19) in (6.20) gives

$$r(\chi; x, z) = w_m^{-1} \int_D dx'dz' G(x, z; x', z') G(x', z'; \chi, 1) + w_c^{-1} \int_C dz' G_{x'}(x, z; 0, z') G_{x'}(0, z'; \chi, 1). \tag{6.21}$$

Finally, the representer kernel defined in (6.11) can be expressed as

$$R(\chi, \eta) = w_m^{-1} \int_D dx'dz' G(\eta, 1; x', z') G(x', z'; \chi, 1) + w_c^{-1} \int_C dz' G_{x'}(\eta, 1; 0, z') G_{x'}(0, z'; \chi, 1). \tag{6.22}$$

As in section 5, the Green's function has a solution in terms of a Fourier cosine series:

$$G(x, z; x', z') = \sum_{n=1}^{\infty} \frac{1}{n\pi} (e^{-n\pi(x+x')} - e^{-n\pi|x-x'|}) \cos n\pi z \cos n\pi z', \tag{6.23}$$

which leads to the following expressions for $r(\chi; x, z)$ and $R(\chi, \eta)$:

$$r(\chi; x, z) = w_m^{-1} \sum_{n=1}^{\infty} \frac{(-1)^n}{2n^2\pi^2} \left[-\left(\frac{1}{n\pi} + (x + \chi)\right) e^{-n\pi(x+\chi)} + \left(\frac{1}{n\pi} + |x - \chi|\right) e^{-n\pi|x-\chi|} \right] \cos n\pi z + w_c^{-1} \sum_{n=1}^{\infty} 2(-1)^n e^{-n\pi(x+\chi)} \cos n\pi z, \tag{6.24}$$

$$R(\chi, \eta) = w_m^{-1} R_m(\chi, \eta) + w_c^{-1} R_c(\chi, \eta), \tag{6.25}$$

where

$$R_m(\chi, \eta) = \sum_{n=1}^{\infty} \frac{1}{2n^2\pi^2} \left[-\left(\frac{1}{n\pi} + (\chi + \eta)\right) e^{-n\pi(\chi+\eta)} + \left(\frac{1}{n\pi} + |\chi - \eta|\right) e^{-n\pi|\chi-\eta|} \right] \tag{6.26}$$

$$R_c(\chi, \eta) = \sum_{n=1}^{\infty} 2e^{-n\pi(\chi+\eta)}. \tag{6.27}$$

With the above expressions for $r(\chi)$ and $R(\chi, \eta)$, the inverse solution $\hat{v}$ is obtained by the inversion of the integral equation (6.10) for the representer coefficients and the evaluation of (6.8). Because the expressions above arising from the weak constraint formulation are more complicated than those arising from the strong constraint, a decomposition into an infinite matrix equation as in section 5 is no longer feasible.

Note how the addition of the model errors has modified the properties of the representer functions. Because of the linearity of the inverse problem, the representer function (6.24) is the sum of two separate terms: the first arising from the errors in the model and the second arising from the errors in the coastal boundary condition. The second term is thus the same as the representer function obtained with the strong constraint formulation in section 5, given by (5.19a). In the limit of infinite model weight, $w_m \to \infty$ the representer function obtained with the weak constraint approaches that obtained with the strong constraint.

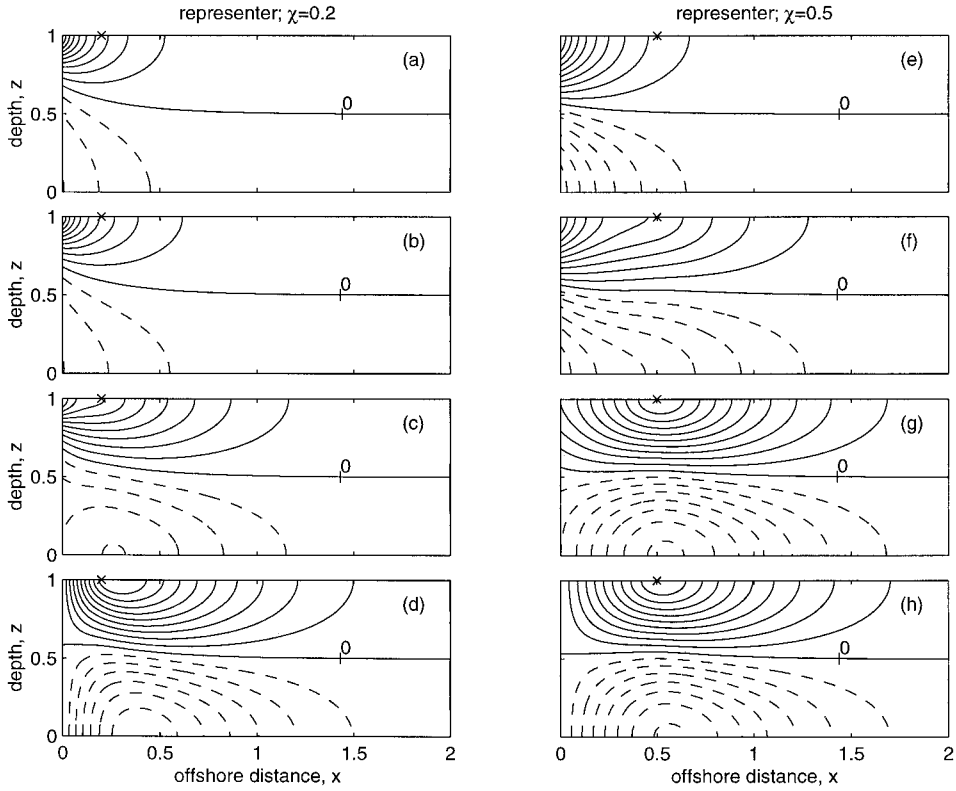

FIG. 1. (Normalized) representer functions for surface data located at an offshore distance of $\chi = 0.2$ (a–d) and $\chi = 0.5$ (e–h), for different values of the ratio of model and coastal boundary condition error weights, w_m/w_c: (a, e) is the strong constraint limit $w_m/w_c \to \infty$, the remainder are for the weak constraint as follows: (b, f) $w_m/w_c = 0.1$; (c, g) $w_m/w_c = 0.01$; (d, h) $w_m/w_c = 0$. Solid lines denote positive values, dashed denote negative, and the contour interval is 0.1 in each case.

7. Properties of the inverse solution

In this section we look at the dependence of the inverse solution on the choice of weights, the data array, and the differences between the strong and weak constraint formulations. Two particular aspects are of interest: the success with which the velocity field at depth can be constructed from the surface data and guidance for the correct choice of weights in the absence of explicit prior error statistics. We examine these both by considering the spectral decomposition of the representer matrices and by constructing suitable twin experiments, in which we use synthetic surface data generated from a known ocean state.

a. Comparison of the strong and the weak formulations

Typical representer functions, as functions of x and z, for the particular cases $\chi = 0.2$ and $\chi = 0.5$, are shown in Fig. 1. The representers also depend on the ratio of the weights w_m and w_c through (6.24). In particular, the special case of the strong constraint, with $w_m/w_c \to \infty$ is shown in Figs. 1a,e, and different examples of the weak constraint are shown in Figs. 1b–d and Figs. 1f–h.

The representers have a useful interpretation: for each data point they tell us where that data point has greatest influence on the inverse solution. Specifically, they may be identified as the covariances of points at the data locations with points in the rest of the domain, when the weights in the penalty functional are taken to be the inverse covariances of the error terms in the undetermined forward model (e.g., Bennett 1992). Using spatially uncorrelated weights, as we do here, corresponds to assuming white noise error covariances in the undetermined forward problem. Although, in general, the weights should contain information about spatial correlations, the use of uncorrelated weights here, and the corresponding reduction in the number of parameters, allows us to illustrate more clearly the properties of the inverse solution.

Consider first the strong constraint. Notice that the greatest influence of the data at χ is on the values of the inverse solution at the coast rather than the values at the data point itself, as might be expected. This is a consequence of the strong constraint of exact model equations, which requires that all solutions must decay exponentially from the coast. Thus the influence of data must necessarily be greatest at the coast. Also notice that for $\chi = 0.2$, that is for a data point near the coast,

the influence of the data on the inverse solution is greater near the surface than at depth, whereas for $\chi = 0.5$ the influence is similar at the surface and at depth. Figures 1a,e have another interpretation. Since the dependence of $r_c(\chi; x, z)$ on x and χ is the same, Fig. 1 can be regarded as the representer function as a function of χ and z for a particular x. This indicates which data locations have the most influence at a given x. Again because of the strong constraint nature of the problem, data located at the coast have the greatest influence on the inverse solution at a given x.

In contrast, the first term in (6.24), multiplied by w_m^{-1}, is plotted in Figs. 1d,h. This can be considered to be the representer function obtained with the weak constraint in the limit of infinite weight given to the coastal boundary condition; that is, $w_c^{-1} \to 0$ so that $\hat{v}(x = 0) \equiv 0$. We see that data at an offshore location now has greatest influence on the inverse solution near that same offshore location. Similarly the inverse solution at an offshore location is most influenced by data near that same offshore location. That the influence of a data point is not maximal at the data point, but farther offshore, results from the constraint $\hat{v}(x = 0) \equiv 0$ together with the required smoothness of the solution.

For intermediate, that is, finite, values of w_m and w_c we obtain a weighted superposition of the two limiting cases. As w_m/w_c increases, data at an offshore location has increasing influence on the inverse solution at the coast, and decreasing influence on the inverse solution at the same off-shore location. Conversely as w_m/w_c decreases, data at an offshore location has decreasing influence on the inverse solution at the coast, and increasing influence on the inverse solution at the same offshore location.

Another clear difference between the two formulations is the offshore decay of the representer. For illustration we consider the representer evaluated at the surface. The strong constraint representer decays on a length scale that approaches π^{-1} as the data point moves farther offshore. This can also be seen from (5.19b), which gives:

$$r(x, 1; \chi) = 2e^{-\pi(x+\chi)} + O(e^{-2\pi(x+\chi)}). \qquad (7.1)$$

Although the weak constraint representer has a similar decay scale for $x \gg \chi \gg 1$, the decay is moderated for $x \sim \chi$ by the term $\exp\{-n\pi|x - \chi|\}$ in the summand of (6.24). Thus data at a given offshore location have a greater horizontal range of influence in the weak constraint formulation than in the strong. Additionally, the decay of the influence in the weak constraint formulation is from the data point, rather than from the coast.

The different properties of the strong and weak formulations can also be investigated by considering the spectral properties of the representer matrix (for the case of discrete data). For definiteness suppose there are N discrete data points, distributed over the surface. The $N \times N$ representer matrix may be interpreted as the covariance matrix of each data point with each other data point, again assuming that the weights chosen in the penalty functional are the inverses of the error covariances in the forward model. Since we are now considering the case of discrete data, the integrals over the surface become sums over the data points. In particular our inverse solution, (6.8) and (6.10), becomes

$$\hat{v} = \mathbf{r}^T(\mathbf{R} + w_d^{-1}\mathbf{I})^{-1}\mathbf{d}, \qquad (7.2)$$

where $\mathbf{d}$ is a vector of length N, $\mathbf{I}$ is the $N \times N$ identity matrix, $\mathbf{r}$ is a vector (of length N) valued function of (x, z), and where matrix multiplication should be understood. We consider the inverse solution evaluated at the data points:

$$\hat{\mathbf{v}} = \hat{v}|_\Delta = \mathbf{R}(\mathbf{R} + w_d^{-1}\mathbf{I})^{-1}\mathbf{d} \qquad (7.3a)$$

$$= \mathbf{Z}\mathbf{\Lambda}(\mathbf{\Lambda} - w_d^{-1}\mathbf{I})^{-1}\mathbf{Z}^T\mathbf{d}, \qquad (7.3b)$$

where $\mathbf{\Lambda}$ is a diagonal matrix composed of the eigenvalues λ_i of $\mathbf{R}$, and $\mathbf{Z}$ is an orthogonal transformation matrix composed of the eigenvectors of $\mathbf{R}$, and such that $\mathbf{R} = \mathbf{Z}\mathbf{\Lambda}\mathbf{Z}^T$. We can write this as

$$\hat{\mathbf{v}} = \text{diag}\left(\frac{\lambda_i}{\lambda_i + w_d^{-1}}\right)\tilde{\mathbf{d}}, \qquad (7.4)$$

where $\tilde{\mathbf{v}} = \mathbf{Z}^T\hat{\mathbf{v}}$ is a vector composed of the projections of $\hat{\mathbf{v}}$ onto the eigenvectors of $\mathbf{R}$, and similarly for $\tilde{\mathbf{d}} = \mathbf{Z}^T\mathbf{d}$. Because of the ill-posed nature of the strong constraint data problem, the condition number of the strong constraint representer matrix is typically very large, increasing for increasing number of data points and tending to infinity in the limit of continuous data. This is reflected in (7.3a) in the ill-posed limit of perfect data, $w_d^{-1} \to 0$, with $\mathbf{R} = \mathbf{R}_c$, the strong constraint representer matrix. To ensure a (strong constraint) inverse solution that depends stably on the data, we therefore require $w_d^{-1} > 0$. Since the λ_i are a rapidly decreasing sequence, the condition that $w_d^{-1} > 0$ therefore means that the right-hand side of (7.4) contributes to the inverse solution only through the largest eigenvalues of $\mathbf{R}$. Further, both the structure of the contribution and the structure of the contributing data is the same as the structure of the eigenvectors associated with these largest eigenvalues because we have projected both the inverse solution and the data onto these eigenvectors.

In light of the above, it is instructive to compare the spectral properties of $\mathbf{R}$ between the strong and the weak formulations. As an example, we use 50 data points distributed evenly from $x = 0.2$ to $x = 1$. Recall that in the weak constraint, $\mathbf{R}$ (6.25) was written as

$$\mathbf{R} = w_m^{-1}\mathbf{R}_m + w_c^{-1}\mathbf{R}_c, \qquad (7.5)$$

with the strong constraint as the limit $w_m^{-1} \to 0$. We first note that the eigenvalues decay much more rapidly in the strong ($\mathbf{R}_c$) than in the weak ($\mathbf{R}_m$) constraint (Figs. 2d–f), which reflects the unstable data dependence of the strong constraint with $w_d^{-1} = 0$. On the other hand, the weak constraint formulation ($w_m^{-1} > 0$) with $w_d^{-1} \to 0$ and $w_c^{-1} \to 0$ does not have the same unstable data

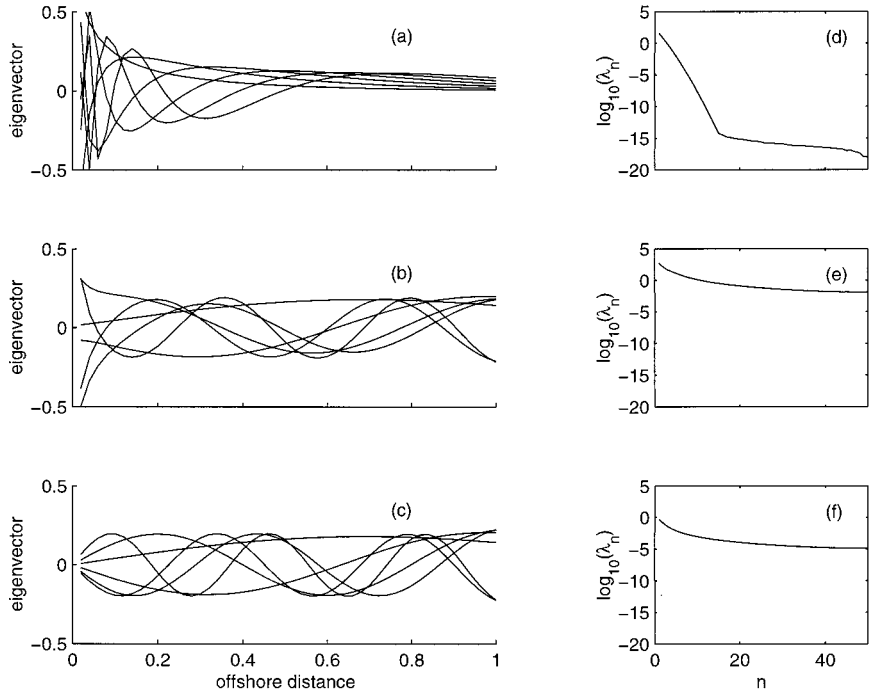

FIG. 2. Eigenvectors (a–c) and eigenvalues (d–f) of the 50 × 50 representer matrix $R = w_m^{-1}R_m + w_c^{-1}R_c$ for the case of 50 data points distributed evenly between $x = 0.02$ and $x = 1$, for different values of w_m/w_c. Values of the weights are (a, d) $w_m/w_c \to \infty$ (strong constraint); (b, e) $w_m/w_c = 0.001$; (c, f) $w_m/w_c = 0$. In (a–c) the first six eigenvectors, associated with the six largest eigenvalues, are plotted. Since the eigenvectors are the same length as the number of data points we identify each component of each vector with a data point, and so the x axis spans the offshore region containing the data points. In (d–f) the logarithm of the decreasing sequence of eigenvalues, $\log(\lambda_n)$ ($n = 1, \cdots, 50$), is plotted.

dependence. Because the eigenvalues decay more rapidly in the strong constraint, the inverse solution contains less horizontal structure: the smaller the eigenvalue, the greater the number of turning points of the corresponding eigenvector. In the weak constraint, the inverse solution can inherit more structure from the data.

Further, in the strong constraint, the largest eigenvectors of $\mathbf{R}_c$ are skewed towards the coast (Fig. 2a), indicating both that the data contributes most information to the inverse solution at the coast and that data located near the coast contribute most to the inverse solution. In the weak constraint, on the other hand, the eigenvectors of $\mathbf{R}_m$ are distributed evenly over the whole data array (Figs. 2b,c). Thus in the weak constraint, data at all locations contribute equally to the inverse solution. An alternative interpretation is that the choice of strong or weak constraint formulation should be dependent on our prior expectations of the spatial structure of the data in that the spatial structure of the eigenvalues of $\mathbf{R}$ should reflect that of the data.

b. *Reconstructing a known ocean state: Twin experiments*

We now consider more explicitly how well the inverse formulation does in recreating a given ocean state from a data sample. That is, we sample a given ocean state and compare the inverse solution obtained from the data with the original ocean state. As a first example we use data sampled from the ''true'' ocean state given by (3.5) in section 3:

$$\mathbf{d} = \upsilon^{(k)}(x, z)|_{\Delta} + \boldsymbol{\delta}, \tag{7.6}$$

with $k = 10$, where Δ is the set of data points, and where $\boldsymbol{\delta}$ is the error associated with the data sampling. Given this data, $\mathbf{d}$, we construct the inverse solution, $\hat{\upsilon}$. We are now interested in how close the inverse solution, $\hat{\upsilon}$, is to the true ocean state, $\upsilon^{(k)}$, that we sampled. Note that $\hat{\upsilon}$, and hence the closeness to $\upsilon^{(k)}$, depends on the choice of model, coastal, and data weights through the ratios w_d/w_m and w_d/w_c, which we donote by γ_{dm} and γ_{dc}, respectively.

One possible quantity to evaluate the closeness to $\upsilon^{(k)}$ is the total squared error, defined as

$$Q = \int_D (\hat{\upsilon} - \upsilon^{(k)})^2. \tag{7.7}$$

Since $Q = Q(\gamma_{\mathrm{dm}}, \gamma_{\mathrm{dc}})$, the minimum of Q with respect to the ratios γ_{dm} and γ_{dc} indicates the best possible reconstruction of $\upsilon^{(k)}$. Note, however, that the minimum does not provide information about which weights we

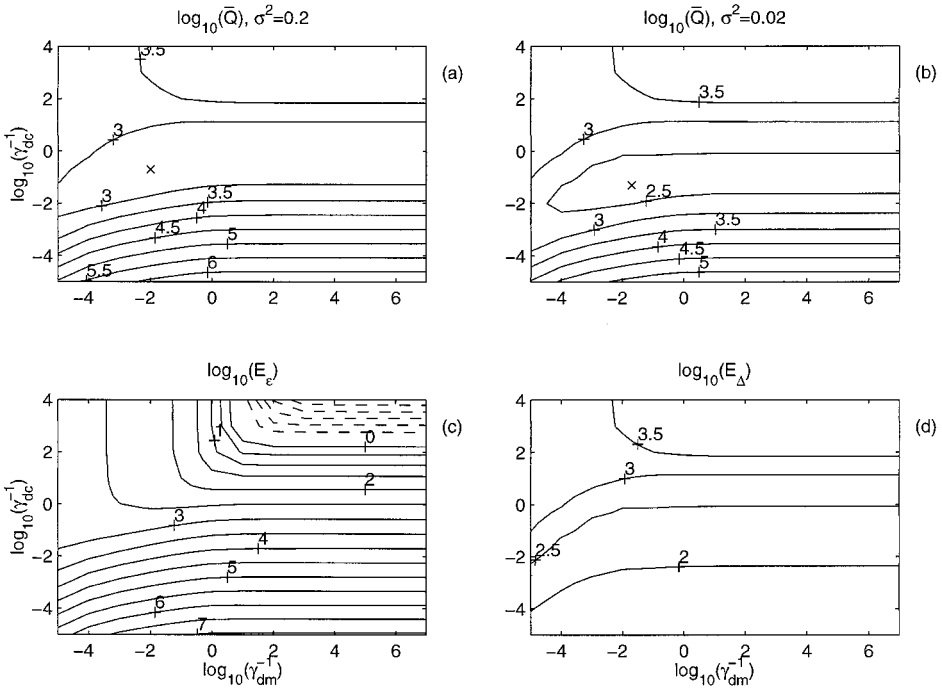

FIG. 3. Plot of $\overline{Q}$, E_ϵ and E_Δ as functions of the ratios γ_{dm} and γ_{dc}, for the case of 50 data points distributed evenly between $x = 0.02$ and $x = 1$, sampled from $v^{(k)}$ with error variance σ^2: (a) $\log_{10}(\overline{Q})$ for $\sigma^2 = 0.2$; (b) $\log_{10}(\overline{Q})$ for $\sigma^2 = 0.02$; (c) $\log_{10}(E_\epsilon)$; (d) $\log_{10}(E_\Delta)$. The x axis is $\log_{10}(\gamma_{dm}^{-1}) = \log_{10}(w_m/w_d)$, the y axis is $\log_{10}(\gamma_{dc}^{-1}) = \log_{10}(w_c/w_d)$, the contour interval is 0.5, and negative contours are dashed. In (a) and (b) the cross depicts the minimum of $\log_{10}(\overline{Q})$.

should choose in a real assimilation situation since it depends upon knowledge of $v^{(k)}$, which is not available.

Since Q also depends upon the particular realization of the data errors, $\boldsymbol{\delta}$, we consider the ensemble average, $\overline{Q}$, with respect to multiple realizations of $\boldsymbol{\delta}$. We assume that $\boldsymbol{\delta}$ is a random, uncorrelated error, with mean $\overline{\boldsymbol{\delta}} = 0$ and uniform variance $\text{var}(\boldsymbol{\delta}) = \sigma^2$. We can write $\overline{Q}$ as the sum of two parts,

$$\overline{Q} = \sigma^2 E_\epsilon + E_\Delta, \tag{7.8}$$

where $E_\epsilon = \int_D e_\epsilon$ and $E_\Delta = \int_D e_\Delta$ are defined by

$$e_\epsilon(x, z) = \text{tr}(\mathbf{P}^{-1}\mathbf{r}\mathbf{r}^{\mathrm{T}}\mathbf{P}^{-1}) \tag{7.9}$$

$$e_\Delta(x, z) = (\hat{v}^0 - v^{(k)})^2, \tag{7.10}$$

with $\mathbf{P} = \mathbf{R} + w_d^{-1}\mathbf{I}$. Recall that $\mathbf{r}$ is a vector valued function of (x, z) of length N, the number of data points, and that $\overline{\boldsymbol{\delta}} = 0$. In (7.10) $\hat{v}^0$ denotes the inverse solution obtained with $\mathbf{d} \equiv v^{(k)}|_\Delta$, that is with $\boldsymbol{\delta} = 0$ in (7.6). The advantage of writing the total error, $\overline{Q}$, as in (7.8), is the separation into a contribution from the data error, E_ϵ, and a contribution from the resolution of the sampling array, E_Δ. Specifically, notice that both E_ϵ and E_Δ are independent of the data and the data error.

First consider the ensemble averaged total error, $\overline{Q}$, which is contoured in Figs. 3a,b for the case of 50 data points spread evenly over [0, 1], with a uniform error variance, σ^2, of 0.2 and 0.02, respectively. For the case $\sigma^2 = 0.2$, we find that $\overline{Q}$ is smallest when the ratios $\gamma_{dm} = 100$ and $\gamma_{dc} = 5$, and for the case $\sigma^2 = 0.02$, we find that $\overline{Q}$ is smallest when the ratios $\gamma_{dm} = 50$ and $\gamma_{dc} = 20$. However, we see that the strong constraint limit, $\gamma_{dm} \to 0$, on the right sides of Figs. 3a,b, gives values of $\overline{Q}$ only slightly larger than the minimum values; that is, the strong constraint does nearly as well as the best weak constraint. That the strong constraint should do so well is perhaps not surprising since the data are sampled from a field that satisfies the model equations exactly and since, by definition, the strong constraint produces an inverse solution that also satisfies the model equations exactly.

The inverse solutions themselves, corresponding to the smallest $\overline{Q}$ for a given data variance, are shown in Fig. 4 for a particular data realization. We can see that for small error variance, $\sigma^2 = 0.02$, the inverse solution $\hat{v}$ is successful at representing $v^{(k)}$, with greater accuracy near the surface than at depth. The inverse solution with larger error variance, $\sigma^2 = 0.2$, is less accurate but still gives a reasonable approximation.

Returning to the decomposition (7.8), we plot E_ϵ and E_Δ in Figs. 3c,d. In the ill-posed limit (strong constraint, perfect data), and with continuous data, E_Δ is identically zero because $\hat{v}^0 \equiv v^{(k)}$, even though the inverse calculation is unstable. Thus the unstable dependence on the data error enters only through the term E_ϵ: for given

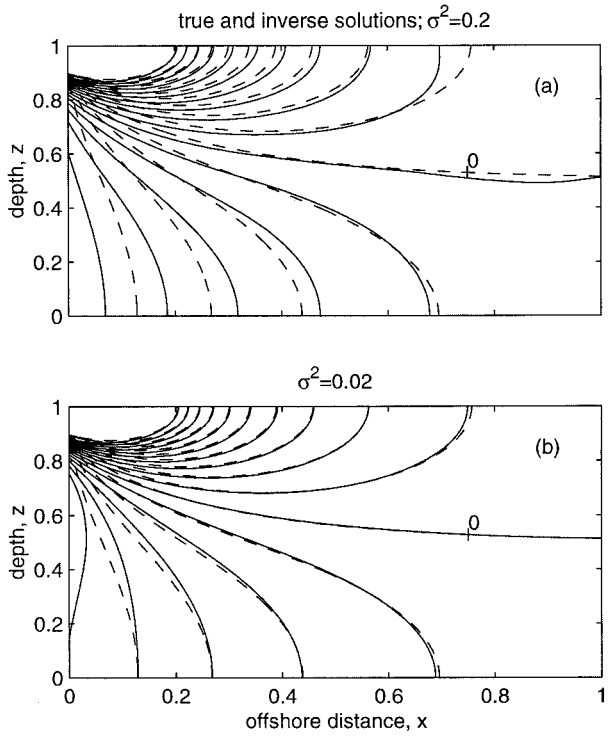

FIG. 4. The true solution, $v^{(k)}$ (dashed), given by (3.5) with $k = 10$ and the inverse solution, $\hat{v}^{\delta}$ (solid), obtained with data taken from $v^{(k)}$ evaluated at the surface with a given error variance, $\sigma^2 = \text{var}(\delta)$. The ratios γ_{dm} and γ_{dc} of the weights used in the inverse calculation are those that give the minimum values of $\overline{Q}$ in Figs. 3a,b. (a) $\sigma^2 = 0.2$, $\gamma_{dm} = 100$, $\gamma_{dc} = 5$; (b) $\sigma^2 = 0.02$, $\gamma_{dm} = 50$, $\gamma_{dc} = 20$. The contour interval is 0.2; contours above the zero contour are positive, those below are negative.

data error variance, σ^2, a large value of the ratio γ_{dc} results in a large value of $\sigma^2 E_\epsilon$ and hence large $\overline{Q}$. Thus knowledge of the data error variance together with (7.8) gives a criterion for selecting the ratio γ_{dc} without the need for knowledge of the coastal boundary error variance. Namely, we choose γ_{dc} so that $\sigma^2 E_\epsilon$ is not too large compared with our prior expectations of the coastal ocean. For discrete data, the ill-posed limit no longer gives $\hat{v}^0 \equiv v^{(k)}$ because some information has been lost due to the sampling resolution. However, we still have approximate equality if there are enough data points, and again the unstable dependence on the data error enters through the term E_ϵ.

To illustrate, we consider the strong constraint, $w_m^{-1} = 0$ so that $\gamma_{dm} = 0$, and plot $e_\epsilon(x, z)$ and $e_\Delta(x, z)$ for different choices of γ_{dc} (Fig. 5). The limit of the ratio $\gamma_{dc} \to \infty$ corresponds to the ill-posed limit. Accordingly, for $\gamma_{dc} = 10^{10}$, we have $e_\epsilon \gg e_\Delta$ everywhere in the domain; that is, the instability due to data error is much greater than the instability due to sampling resolution. Further, the spatial structure of e_ϵ indicates that the solution is most unstable at the coast. For smaller $\gamma_{dc} = 10^2$, e_ϵ is smaller but it retains a similar spatial structure. In the other limit, that of worthless data with the ratio $\gamma_{dc} \to 0$, we can show that $e_\epsilon \to 0$ and that $e_\Delta \to (v^{(k)})^2$. Thus there is some intermediate range of γ_{dc} where $\sigma^2 E_\epsilon$ and E_Δ are of similar magnitude and it is for γ_{dc} in this range that we obtain the minimum of $\overline{Q}$. The interpretation is that E_Δ represents the least error achievable given exact data, for a given choice of γ_{dc}. On the other hand, E_ϵ represents the stability of the dependence of the solution on the data errors, again for a given choice of γ_{dc}.

As a concrete example of how well the inverse solution can reproduce the true state, $v^{(k)}$, we have taken one particular data realization, with a given error variance, and have compared contour plots of $\hat{v}$ and $v^{(k)}$ for the values of w_c and w_m that give the least $\overline{Q}$ for that error variance (Fig. 4). This has the disadvantage of being dependent on the random data error (because $\hat{v}$ is). An alternative approach is to consider the mean squared error, $\overline{q} = \overline{(\hat{v} - v^{(k)})^2}$, which is plotted as a function of (x, z) in Fig. 6. The cases corresponding to Fig. 4 are shown in Figs. 6a,b with 50 data points and data error variances of $\sigma^2 = 0.2$ and $\sigma^2 = 0.02$. It is seen that the maximum error in the inverse solution occurs near the coast and near the surface. Figures 6c,d show the mean squared error, $\overline{q}$, for the case of 10 data points, again with data error variance $\sigma^2 = 0.2$ and $\sigma^2 = 0.02$. The pattern of the errors is the same but values are generally larger, especially in the case of $\sigma = 0.2$. In both cases with 50 and 10 data points, the minimum of $\overline{Q}$ is obtained for larger values of γ_{dc} and smaller values of γ_{dm} when the error variance is smaller (better data). Further, in the case of $\sigma^2 = 0.2$ (noisy data) the higher, $N = 50$, data resolution requires smaller values of γ_{dc} and γ_{dm} or, equivalently, a smaller data weight w_d, as expected from consideration of (7.2).

Finally we consider assimilating data that is sampled from an ocean state that does not satisfy the model equations exactly. For example, consider v^{α}, that is a solution to

$$v_{xx} + \alpha v_{zz} = 0, \tag{7.11}$$

together with the boundary conditions (3.2) satisfied by $v^{(k)}$ in section 3. Such a situation could arise, e.g., from an incorrect choice of the stratification parameter, S. We proceed as above by sampling v^{α} to give data, $\mathbf{d} = v^{\alpha}|_\Delta + \boldsymbol{\delta}$, and constructing the inverse solution, $\hat{v}^{\alpha\delta} = \mathbf{r}^{\mathrm{T}}\mathbf{P}^{-1}\mathbf{d}$. The contribution to $\overline{Q}^{\alpha}$ from E_ϵ is the same as before, depending only upon the representers and the error weights. The contribution from E_Δ is different, however, depending upon both v^{α} and $\hat{v}^{\alpha\delta}$. The dependence of $\overline{Q}^{\alpha}$ on the model weight, coastal boundary condition weight, and data weight, through the ratios γ_{dm} and γ_{dc}, is shown in Fig. 7 for different values of data error variance, σ^2 with the special case $\sigma^2 = 0$ corresponding to the field E_Δ. There is now a clear minimum in E_Δ for $w_m \propto \gamma_{dm}^{-1} < \infty$, and therefore also in $\overline{Q}^{\alpha}$ for small values of σ^2. That is, the improvement of the weak constraint over the strong constraint is significantly greater here than previously when the data

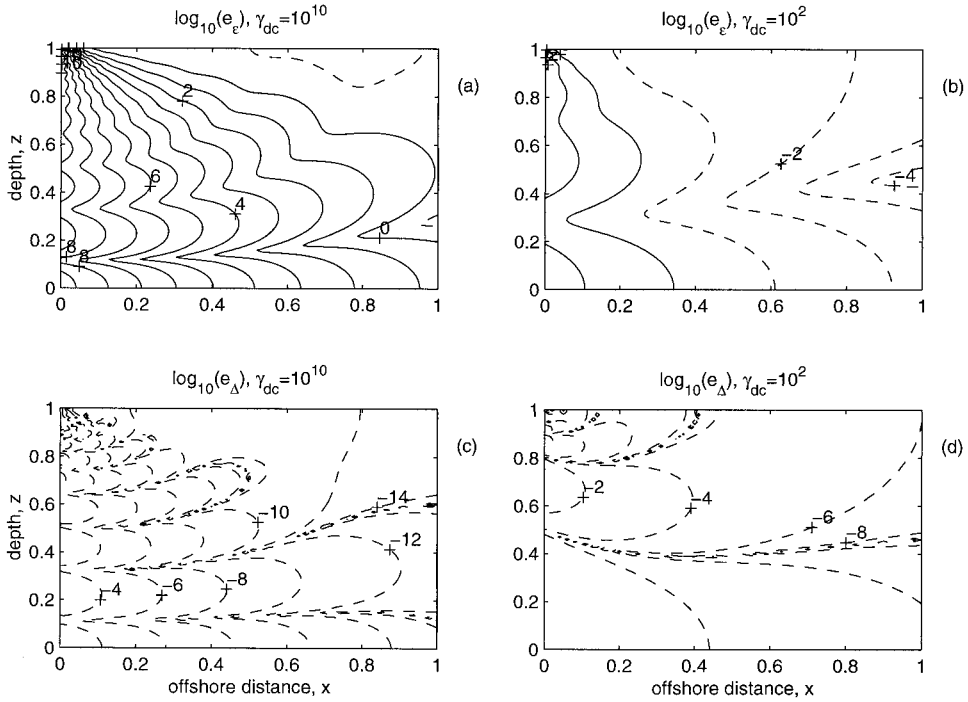

FIG. 5. Plot of e_ϵ and e_Δ as functions of (x, z), for the case of 50 data points distributed evenly between $x = 0.02$ and $x = 1$ sampled from $\upsilon^{(k)}$, in the strong constraint limit, $\gamma_{dm} = 0$, and for different values of γ_{dc}: (a) $\log_{10}(e_\epsilon)$ for $\gamma_{dc} = 10^{10}$; (b) $\log_{10}(e_\epsilon)$ for $\gamma_{dc} = 100$; (c) $\log_{10}(e_\Delta)$ for $\gamma_{dc} = 10^{10}$; (d) $\log_{10}(e_\Delta)$ for $\gamma_{dc} = 100$. The contour interval is 1 in (a, b) and 2 in (c, d); negative contours are dashed.

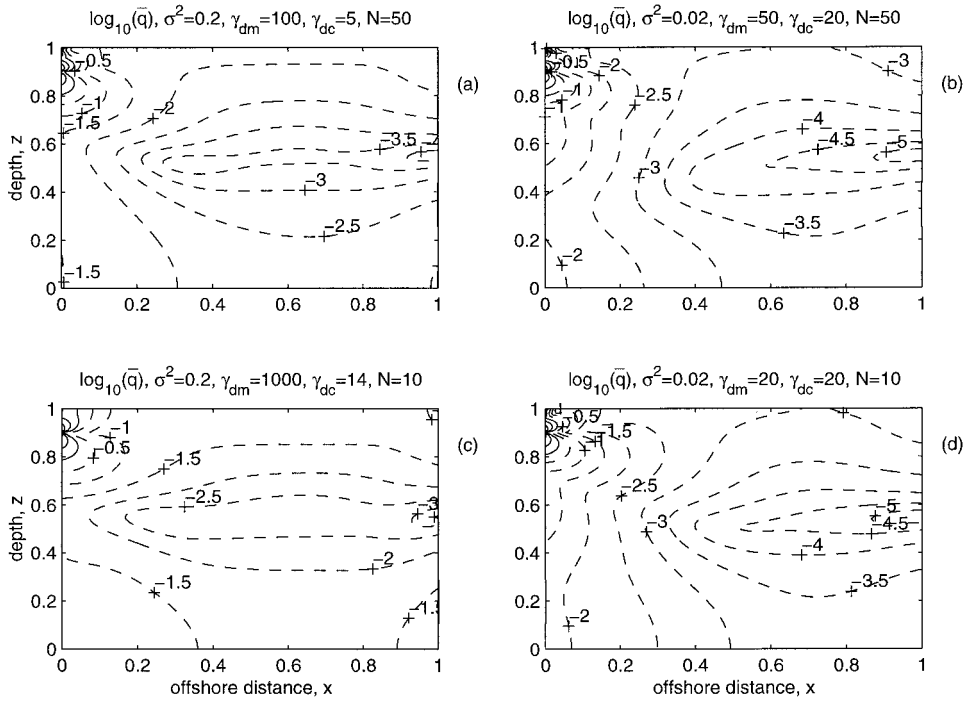

FIG. 6. Plot of $\overline{q}$ as a function of (x, z), for the cases of 50 data points distributed evenly between $x = 0.02$ and $x = 1$ (a, b), and 10 data points distributed evenly between $x = 0.1$ and $x = 1$ (c, d). The values of γ_{dm} and γ_{dc} are those that give the minimum values of $\overline{Q}$ in each case. (a) 50 data points, $\sigma^2 = 0.2$, $\gamma_{dm} = 100$, $\gamma_{dc} = 5$; (b) 50 data points, $\sigma^2 = 0.02$, $\gamma_{dm} = 50$, $\gamma_{dc} = 20$; (c) 10 data points, $\sigma^2 = 0.2$, $\gamma_{dm} = 1000$, $\gamma_{dc} = 14$; (d) 10 data points, $\sigma^2 = 0.01$, $\gamma_{dm} = 20$, $\gamma_{dc} = 20$. The contour interval is 0.5 and negative contours are dashed.

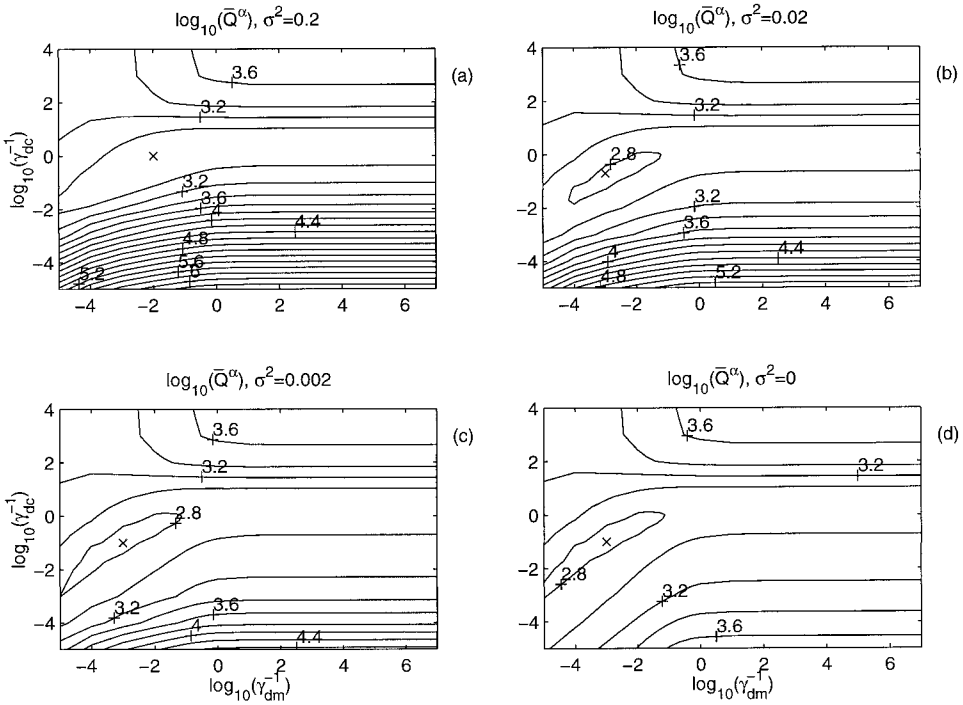

FIG. 7. Plot of $\overline{Q}^{\alpha}$, for $\alpha = 1.5$, as a function of the ratios γ_{dm} and γ_{dc}, for the case of 50 data points distributed evenly between $x = 0.02$ and $x = 1$, sampled from v^{α} with error variance σ^2: (a) $\sigma^2 = 0.2$; (b) $\sigma^2 = 0.02$; (c) $\sigma^2 = 0.002$; (d) $\sigma^2 = 0$. The x and y axes are as in Fig. 3; the contour interval is 0.2. The cross depicts the minimum of $\log_{10}(\overline{Q}^{\alpha})$.

was sampled from $v^{(k)}$. The true and the inverse velocity fields themselves are shown in Fig. 8, for $\alpha = 1.5$ and $\sigma^2 = 0.02$, for both the weak constraint minimum, $\gamma_{dm}^{-1} = 0.001$, $\gamma_{dc}^{-1} = 0.2$, and the strong constraint minimum, $\gamma_{dm}^{-1} \to \infty$, $\gamma_{dc}^{-1} = 2$, illustrating the improvement of the weak constraint over the strong. Note that here the inverse solutions are less successful than when the data was sampled from an exact solution of the model equations (Fig. 4).

8. Conclusions

We have used a highly idealized, linear, primitive equation model together with an optimal, variational data assimilation scheme, to evaluate the extraction of a z-dependent flow field from surface type data. With the physical simplifications made, the forward model and inverse model can be formulated in terms of the alongshore velocity alone, so attention is restricted to the assimilation of a surface alongshore velocity field. We have for the present left aside the issues associated with the relation of the alongshore and across-shore surface currents and with errors in the solution of a mixed layer model to obtain the velocity field below the surface boundary layer.

Our assimilation scheme uses an inverse formulation to find the best fit to the model, to the coastal boundary condition, which represents our knowledge of the open ocean, and to the data. Without this inverse formulation, simply replacing the coastal boundary condition with an extra boundary condition consisting of the data results in an ill-posed problem. The ill-posedness is manifested in the sensitive dependence of the solution at depth upon the surface data. The inverse formulation illustrates explicity how the ill-posedness is resolved: through the regularization of an ill-conditioned linear operator, whose inverse is a linear transformation from the data to the solution at depth.

The inverse solution is constructed as a linear combination of representer functions, with one representer function for each data point. These representers can be regarded as covariances between points in the domain interior and surface data points. Thus they indicate the influence of the surface data on the inverse solution at depth. It turns out that in both the strong and in the weak constraint inverse formulations there is considerable influence at depth. In the case of the strong constraint, however, it is shown that the greatest data influence is always at the coast, a result of the restriction that solutions to the exact model equations decay exponentially at infinity, in turn consistent with our separation into inner and outer regions. On the other hand, in the case of the weak constraint the data has greatest influence on the inverse solution close to the data point, which is intuitively more reasonable. Thus we expect a weak constraint formulation to be most successful in

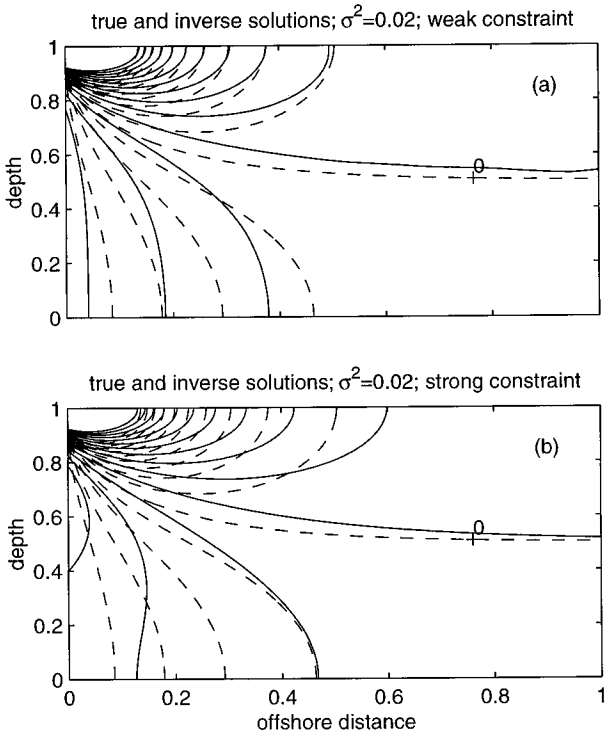

FIG. 8. The true solution, v^{α} (dashed), that solves (7.11) for $\alpha = 1.5$, and the inverse solution, $\hat{v}^{\alpha\delta}$ (solid), obtained with data taken from v^{α} evaluated at the surface with a given error variance, $\sigma^2 = \text{var}(\delta) = 0.02$: (a) $\gamma_{dm}^{-1} = 0.001$ and $\gamma_{dc}^{-1} = 0.2$, corresponding to the minimum of $\overline{Q}^{\alpha}$ in Fig. 7b; (b) $\gamma_{dm}^{-1} \to \infty$ and $\gamma_{dc}^{-1} = 2$, corresponding to the minimum of $\overline{Q}^{\alpha}$ restricted to the strong constraint. The contouring is as in Fig. 4.

general because the anomalously large data influence at the coast is modified.

In the case of the strong-constraint inverse formulation our inverse solution depends on a single parameter, the ratio of the data weight to the coastal boundary condition weight. In the case of the weak constraint, in which there are model errors, our inverse solution depends on two parameters, the ratios of the data weight both to the coastal boundary condition weight and to the model weight. In each case the dependence on these parameters is shown explicitly. For our inverse formulation to be used as a hypothesis testing model, the weights should be chosen according to prior estimates of the error covariances of the data, model, and boundary condition, derived from our assumptions about the forward model and our knowledge of the real ocean. However, in the absence of such estimates of error covariances, our inverse solution, regarded as a function of the weights, can be compared with the features that we expect a simplified coastal ocean to possess, and the comparison can be used as guidance for selecting weights. Although no prior estimates of error covariances are made, our choice of weights is still based on prior knowledge of the ocean state and, therefore, based on the same information that is available for estimating error covariances.

The above approach is particularly useful in this study because of the analytic forms of the solution and of the representer functions. Spectral decomposition of the representer matrix illustrates the influence of the data on the solution as a function of data location. Considering the eigenvectors in the weak constraint case suggests a ratio of the model weight to the coastal boundary condition weight, which ultimately depends upon our prior knowledge of the relative influence of the data on the interior and coastal boundary fields.

Similarly, twin experiments make use of the analytic expressions for the representer functions and representer matrix. When we consider a simple measure of the success of the inverse solution as the squared difference between the inverse solution and true ocean state, a decomposition is possible into contributions from the data error (E_{ϵ}) and from the sampling resolution (E_{Δ}). In the particular case when the true ocean state is an exact solution to our model equations, the contribution from the sampling resolution is small: most of the departure of the inverse solution is from errors in the data. Again, prior knowledge of the typical spatial structure of a simplified coastal ocean and comparison with the spatial structure of E_{ε} leads to a suggested value of the model and coastal boundary condition weights.

In the case when the true ocean state is an exact solution to our model equations, the strong constraint inverse formulation does nearly as well as the weak constraint, provided the data error variance is not too large. On the other hand, when the true ocean state is not an exact solution, the weak constraint gives a significant improvement over the strong constraint. In our example the second ocean state was given by assuming an error in our estimate of the stratification parameter, but alternatives could also be given by including dynamics neglected in our simple model. Thus, except in the unlikely case that the data is sampled from an ocean state that closely fits the dynamical model, a weak constraint formulation is necessary to provide an accurate inverse solution.

Acknowledgments. This research was supported by the Office of Naval Research (ONR) Ocean Modeling and Prediction Program under Grant N00014-98-1-0043 and also by the ONR Coastal Dynamics Program under Grant N00014-93-1-1301.

APPENDIX A

Solution of the Inverse Problem by Fourier Expansion: The "Poor Man's Inverse"

Here we outline an alternative minimization approach that gives (5.28) more directly. For brevity we only report the procedure for the strong constraint problem but a similar prcedure can be applied to the weak con-

straint, replacing the a_n below with $a_n(x)$. Instead of taking the variational derivative of the penalty functional $\mathcal{T}[v]$ immediately, we first pose a Fourier series expansion for $v(x, z)$. This is possible because we require the governing equation, $\nabla^2 v = 0$, and boundary conditions $v_z = 0$ at $z = 0, 1$ to be satisfied exactly. The functional dependence of $\mathcal{T}[v]$ on v now becomes an ordinary dependence on the Fourier coefficients, a_n of v, so that $\mathcal{T} = \mathcal{T}[a_n]$, $n = 1, 2, \cdots$, say. Minimization of this penalty function is then achieved by requiring that all partial derivatives with respect to the Fourier coefficients equal zero.

Suppose there is an undetermined Fourier series expansion for v,

$$v(x, z) = \sum_{n=1}^{\infty} a_n e^{-n\pi x} \cos n\pi z. \tag{A.1}$$

We want to choose the coefficients to minimize $\mathcal{T} = \mathcal{T}[a_n]$, where

$$\mathcal{T}[a_n] = w_c \int_0^1 dz'(v(0, z'))^2 + w_d \int_0^\infty d\chi(v(\chi, 1) - d(\chi))^2, \tag{A.2}$$

$$= w_c \int_0^1 dz' \left(\sum_{n=1}^{\infty} a_n \cos n\pi z' \right)^2 + w_d \int_0^\infty d\chi \left(\sum_{n=1}^{\infty} a_n e^{-n\pi\chi}(-1)^n - d(\chi) \right)^2. \tag{A.3}$$

Setting all partial derivatives with respect to the a_n equal to zero,

$$\frac{\partial \mathcal{T}[a_n]}{\partial a_m} = 0 \tag{A.4}$$

gives

$$w_c \int_0^1 dz' \cos m\pi z' \left(\sum_{n=1}^{\infty} a_n \cos n\pi z' \right) + w_d \int_0^\infty d\chi e^{-m\pi\chi}(-1)^m \times \left(\sum_{n=1}^{\infty} a_n e^{-n\pi\chi}(-1)^n - d(\chi) \right) = 0. \tag{A.5}$$

Rearranging and setting $\overline{v}_n = a_n(-1)^n$, (A.5) becomes

$$\sum_{n=1}^{\infty} \left[\frac{1}{(m + n)} + \frac{\pi}{2} c\delta_{mn} \right] \overline{v}_n = \pi \int_0^\infty d\chi d(\chi) e^{-m\pi\chi}, \tag{A.6}$$

which is the same as (5.27).

We now justify why it is possible to treat the baroclinic part of the inverse problem separately from the barotropic part, both in the above formulation and in the main text. Suppose the barotropic part of the velocity and of the data is retained. Then the representation (A.1) has an extra term, $a_0 = \text{const}$, in the summand representing the barotropic field. Also the data will, in general, be nonvanishing at large x. For simplicity, we assume that data is provided out to an offshore distance L, where $L \gg 1$, that is large compared with the baroclinic Rossby radius.

The penalty functional now has the form

$$\mathcal{T}[a_n] = w_c \int_0^1 dz' \left(a_0 + \sum_{n=1}^{\infty} a_n \cos n\pi z' \right)^2 + w_d \int_0^L d\chi \left(a_0 + \sum_{n=1}^{\infty} a_n e^{-n\pi\chi}(-1)^n - d(\chi) \right)^2. \tag{A.7}$$

Setting the partial derivative with respect to a_0 to zero then gives

$$w_c a_0 + w_d \int_0^L d\chi \times \left(a_0 + \sum_{n=1}^{\infty} a_n e^{-n\pi\chi}(-1)^n - d(\chi) \right) = 0, \tag{A.8}$$

which in the limit $L \gg 1$ gives

$$a_0 = \overline{d} + O(L^{-1}), \tag{A.9}$$

where

$$\overline{d} = \frac{1}{L} \int_0^L d\chi d(\chi). \tag{A.10}$$

In other words, the barotropic part of the inverse solution is given approximately by the cross-shore average of all the data. The remainder of the inverse calculation then procedes as before but with the barotropic term $\overline{d}$ subtracted from each original data value, that is with

$$d(\chi) \to d(\chi) - \overline{d}. \tag{A.11}$$

APPENDIX B

Construction of the Inverse Solution

We outline the procedure for finding the minimum of a penalty functional $\mathcal{T}$ of the form

$$\mathcal{T}[v] = (v, v) + w_d \int_S (v - d)^2. \tag{B.1}$$

where $(\cdot\,, \cdot)$ is an inner product over a Hilbert space H of admissible functions. The procedure is the same as given in Bennett (1992, Chapter 5) except that the second term in (B.1) is an integral over a continuous set of data points, S, instead of a sum over a discrete set.

The Riesz representation theorem states that, for each $\chi \in S$, and for each $v \in H$, there exists a unique function r_χ (belonging to H) such that

$$v|_\chi = (r_\chi, v), \tag{B.2}$$

where $v|_\chi$ denotes the value of the function v evaluated at the point $\chi \in S$ (e.g., Renardy and Rogers 1993, section 6.3), and $r_\chi = r(\chi; x, z)$. (Here and in the following we use Greek subscripts to indicate the dependence on points in S.) With r so defined the penalty functional, $\mathcal{T}$, can be written

$$\mathcal{T}[v] = (v, v) + w_d \int_S ((v, r_\chi) - d)^2. \tag{B.3}$$

An arbitrary $v \in H$ can always be written in the form

$$v = \int_S v_\chi r_\chi + g \tag{B.4}$$

for some numbers (representer coefficients) ν_χ and some function $g \in H$ orthogonal to all the r_χ that satisfies $(r_\chi, g) = 0$ for all $\chi \in S$. Substituting (B.4) into (B.3) and simplifying gives

$$\mathcal{T} = \int_{S_\chi}\int_{S_\eta} \nu_\chi R_{\chi\eta}\nu_\eta + w_d \int_{S_\chi}\int_{S_\eta}\int_{S_\zeta} (R_{\chi\eta}\nu_\eta - d_\chi)(R_{\chi\zeta}\nu_\zeta - d_\chi) + (g, g), \tag{B.5}$$

where

$$R_{\chi\eta} = (r_\chi, r_\eta) = r_\chi|_\eta. \tag{B.6}$$

Since $(g, g) \geq 0$ for any g, $\mathcal{T}$ is least when $(g, g) = 0$, which is true if, and only if, $g = 0$. Completing the square of (B.5) (and setting $g = 0$) gives

$$\mathcal{T} = \int_{S_\chi}\int_{S_\eta} (\nu_\chi - \hat{\nu}_\chi)\left(R_{\chi\eta} + w_d \int_{S_\zeta} R_{\chi\zeta}R_{\zeta\eta}\right)(\nu_\eta - \hat{\nu}_\eta) - \int_{S_\chi}\int_{S_\eta} \hat{\nu}_\chi\left(R_{\chi\eta} + w_d \int_{S_\zeta} R_{\chi\zeta}R_{\zeta\eta}\right)\hat{\nu}_\eta + w_d \int_{S_\chi} d_\chi d_\chi, \tag{B.7}$$

where $\hat{\nu}$ is defined by

$$\int_{S_\chi}\left(R_{\chi\eta} + w_d \int_{S_\zeta} R_{\chi\zeta}R_{\zeta\eta}\right)\hat{\nu}_\chi = w_d \int_{S_\chi} R_{\chi\eta}\, d_\chi. \tag{B.8}$$

Hence $\mathcal{T}$ is least when $\nu = \hat{\nu}$, that is, when

$$\nu_\chi + w_d \int_{S_\eta} R_{\chi\eta}\nu_\eta = w_d d_\chi, \tag{B.9}$$

or equivalently,

$$\int_{S_\eta} (R_{\chi\eta} + w_d^{-1}\delta(\chi - \eta))\nu_\eta = d_\chi. \tag{B.10}$$

This is the eq, (5.15) and (6.10) given in sections 5 and 6, for the representer coefficients ν that minimize $\mathcal{T}$.

Another approach to finding the minimum of $\mathcal{T}$ is to use the calculus of variations to take the functional derivative of (B.1) and solve the resulting Euler–Lagrange equations, in our case,

$$\nabla^2 v = w_m^{-1}\lambda \tag{B.11a}$$

$$\nabla^2\lambda = -w_d[\delta(1 - z) - 1](v(x, 1) - d) \tag{B.11b}$$

$$v = -w_c^{-1}\lambda_x \quad \text{at } x = 0, \qquad v \to 0 \quad \text{at } x \to \infty,$$
$$v_z = 0 \qquad \text{at } z = 0, 1; \tag{B.12a}$$

$$\lambda = 0 \qquad \text{at } x = 0, \qquad \lambda \to 0 \quad \text{at } x \to \infty,$$
$$\lambda_z = 0 \qquad \text{at } z = 0, 1, \tag{B.12b}$$

where we have defined the adjoint variable, λ, by $\lambda = w_m\varphi$ and where $\varphi = \nabla^2 v$ represents the model errors. Note that the strong constraint Euler-Lagrange equations are obtained by taking the limit $w_m \to \infty$. One way to solve (B.11a,b) with (B.12a,b) is to consider the following system for $s(\chi; x, z)$ and $s^\dagger(\chi; x, z)$:

$$\nabla^2 s = w_m^{-1}s^\dagger \tag{B.13a}$$

$$\nabla^2 s^\dagger = [\delta(1 - z) - 1]\delta(\chi - x) \tag{B.13b}$$

$$s = -w_c^{-1}s_x^\dagger \quad \text{at } x = 0, \qquad s \to 0 \quad \text{at } x \to \infty,$$
$$s_z = 0 \qquad \text{at } z = 0, 1; \tag{B.14a}$$

$$s^\dagger = 0 \qquad \text{at } x = 0, \qquad s^\dagger \to 0 \quad \text{at } x \to \infty,$$
$$s_z^\dagger = 0 \qquad \text{at } z = 0, 1, \tag{B.14b}$$

and to show, by standard manipulation that the solution $\hat{v}$ of (B.11a,b) can be written as a superposition of solutions s of (B.13a,b). That is $\hat{v}$ is of the form

$$\hat{v}(x, z) = \int_0^\infty d\chi\alpha(\chi)s(\chi; x, z). \tag{B.15}$$

In fact, the functions $s(\chi; x, z)$ are the same as the functions r_χ defined in (B.2) [when the inner product is defined as in (6.6)], which is seen as follows. Defining $w_m^{-1}r_\chi^\dagger = \nabla^2 r_\chi$, we have, for arbitrary v

$$\upsilon|_\chi = (r_\chi, \upsilon) = w_m \int_D \nabla^2 r_\chi \nabla^2 \upsilon + w_c \int_C r_\chi \upsilon$$

$$= \int_D r_\chi^\dagger \nabla^2 \upsilon + w_c \int_C r_\chi \upsilon \qquad \text{(B.16)}$$

and, additionally,

$$\upsilon|_\chi = \int_D \delta(\chi - x)[\delta(1 - z) - 1]\upsilon(x, z). \qquad \text{(B.17)}$$

Integrating (B.16) by parts and equating the result with the right hand side of (B.17), and using the fact that υ is arbitrary, shows that r and $r^\dagger$ satisfy a system of equations and boundary conditions identical to (B.13a,b) and (B.14a,b). Thus, (B.13a,b), provide a means of obtaining the representer functions r_χ defined by (B.2).

APPENDIX C

Alternative Model Errors in the Weak Constraint Formulation

Since the analysis of sections 5 and 6 was concerned only with reconstructing a given alongshore velocity field it was natural to only consider errors in the equation $\nabla^2 \upsilon = 0$. A more thorough approach, and one which allows reconstruction of the other fields, is to return to the original approximate equations (2.12a–e) and include error terms to represent the terms neglected by scaling arguments. For example, we might assume that the greatest source of model error occurs in the horizontal momentum equations (2.12a,b), and in the thermodynamic equation, (2.12c), and that the continuity and hydrostatic equations, (2.12d,e) are exact. Considering only the inner, coastal region as above, we obtain from (2.12a–e) the following equations:

$$\rho_z - \upsilon_x = \varphi_1, \qquad \text{(C.1a)}$$

$$\rho_x + \upsilon_z = \varphi_2, \qquad \text{(C.1b)}$$

where ρ is the density and where φ_1 and φ_2 represent nonlinear and other small terms neglected in the derivation of $\nabla^2 \upsilon = 0$ in section 3. The inverse solution is then the solution $(\hat{\rho}, \hat{\upsilon})$ that minimizes the penalty functional defined by

$$\mathcal{T}[\rho, \upsilon] = w_m \int_D (\varphi_1^2 + \varphi_2^2) + w_c \int_C \varepsilon^2$$

$$+ w_d \int_S \delta^2, \qquad \text{(C.2)}$$

subject to the appropriate boundary conditions. Here w_m is the weight associated with the model errors. Given $(\hat{\rho}, \hat{\upsilon})$ the remaining fields can then be calculated.

Problems occur, however in the use of (C.2) because we are minimizing the norm of a gradient, namely the gradients of ρ and υ, and the norm of the model–data misfit, with data that is given on the boundary and using weights that are singular in their spatial influence. This can lead to the unwanted situation where the functions that minimize (C.2) do not belong to the class of admissible functions for our problem, for example, they are either not continuous or are inconsistent with the boundary conditions. This could be resolved, for example, by an additional term in the penalty functional that penalizes discontinuities, or by using a model weight that is spatially dependent.

REFERENCES

Allen, J. S., 1973: Upwelling and coastal jets in a continuously stratified ocean. *J. Phys. Oceanogr.*, **3,** 245–257.

Bennett, A. F., 1992: *Inverse Methods in Physical Oceanography.* Cambridge University Press, 346 pp.

Choi, M.-D., 1983: Tricks or treats with the Hilbert matrix. *Amer. Math. Mon.,* **90,** 301–312.

Hadamard, J., 1952: *Lectures on Cauchy's Problem in Linear Partial Differential Equations.* Dover, 316 pp.

Kosro, P. M., J. A. Barth, and P. T. Strub, 1997: The coastal jet: Observations of surface currents over the Oregon continental shelf from HF radar. *Oceanography,* **10,** 53–56.

Lewis, J. K., I. Shulman, and A. F. Blumberg, 1998: Assimilation of Doppler radar current data into numerical ocean models. *Contin. Shelf Res.,* **18,** 541–559.

Paduan, J. D., and H. C. Graber, 1997: Introduction to high-frequency radar: Reality and myth. *Oceanography,* **10,** 36–39.

Pedlosky, J., 1987: *Geophysical Fluid Dynamics.* Springer-Verlag, 910 pp.

Renardy, M., and R. C. Rogers, 1993: *An Introduction to Partial Differential Equations.* Springer-Verlag, 488 pp.